energies

MDPI

Review

Multiphase Motors and Drive Systems for Electric Vehicle Powertrains: State of the Art Analysis and Future Trends

Mohamed Amine Frikha [1,2], Julien Croonen [1,2], Kritika Deepak [1,2], Yassine Benômar [1,2,*], Mohamed El Baghdadi [1,2] and Omar Hegazy [1,2,*]

[1] MOBI-EPOWERS Research Group, ETEC Department, Vrije Universiteit Brussel (VUB), 1050 Brussels, Belgium
[2] Flanders Make, Gaston Geenslaan 8, 3001 Heverlee, Belgium
* Correspondence: yassine.benomar@vub.be (Y.B.); omar.hegazy@vub.be (O.H.)

Abstract: Multiphase drives (MPDs) have been the subject of research for the last two decades. Despite being a technology that is still in the process of development, a significant number of research studies and developments have been reported in scientific literature over the past few years. This article aims to collect and present a review of these recent contributions, providing a comprehensive and insightful state of the art on this topic and future technology trends. The elaborated aspects include the advantages of multiphase machines, a general introduction to five-phase and six-phase machines, and their modelling techniques. In addition, new promising MPD topologies are covered. Recent advances in modulation techniques and the control of multilevel converters are also discussed. Finally, future trends and challenges in further developing this technology are discussed.

Keywords: electric vehicles; multiphase drives; multiphase machines; five-phase machines; six-phase machines; modelling; control

Citation: Frikha, M.A.; Croonen, J.; Deepak, K.; Benômar, Y.; El Baghdadi, M.; Hegazy, O. Multiphase Motors and Drive Systems for Electric Vehicle Powertrains: State of the Art Analysis and Future Trends. *Energies* **2023**, *16*, 768. https://doi.org/10.3390/en16020768

Academic Editor: Chunhua Liu

Received: 30 November 2022
Revised: 4 January 2023
Accepted: 5 January 2023
Published: 9 January 2023

1. Introduction

As the demand for electric vehicles (EVs) and sustainable mobility grows globally [1], multiphase drives (MPDs) are finding increased attention in industry and academia as one of the preferred choices of power conversion systems. The MPD was first introduced in [2] and dedicated to a five-phase induction machine. The six-phase induction machine is studied in [3] as another milestone in the development of MPDs. In their origin, multiphase machines were used mainly for electrical power generation, as presented in [4], but nowadays, they seem suitable for high-power applications. Moreover, the evolution in power semiconductor devices and the advancement of converter modulation techniques have motivated more and more research on the topic of MPDs. The characteristics of MPDs have drawn researchers to utilise them in industrial and traction applications where fault-tolerant capability is a crucial design feature, such as electric vehicles [5–7], marine propulsion [8–13], and aerospace [14].

Recently, there have been several attempts to review the current state of MPDs in the literature [15,16]. However, most papers focused on six-phase machines. This paper aims to provide a more comprehensive overview of recent developments in the field by covering a wide range of multiphase topologies, including five-phase, six-phase, multiples of three, seven, and nine-phase drives. These topologies are compared and summarised in simple tables, and the paper also discusses recent modelling, modulation, and control techniques. Additionally, the paper examines the current status of industrialised MPDs in the market and discusses challenges and future trends in the field.

In addition, multiphase drives offer many outstanding merits over conventional three-phase drives [17–20], including less per-phase current or voltage; the stator excitation in a multiphase machine produces improved magnetomotive force (MMF), resulting in lower space harmonics, lower torque ripples, and higher efficiency than in

three-phase drives. Such excitation produces pulsating torques at even multiples of the fundamental excitation frequency [21]. Furthermore, using MPDs reduces dc-link harmonics, decreases the necessary dc-link capacitance, and improves fault-tolerant operation because the degrees of freedom increase as the number of independent phases increases [22–28]. In other words, if one phase of a three-phase machine becomes open-circuited, the machine becomes two-phase. It may continue to run, but it requires some external means for starting and must be operated in a highly regulated manner. To illustrate, if one phase of a 15-phase machine becomes open-circuited, it will still self-start and will run with only minimal de-rating. These characteristics of MPDs are of particular importance for EV applications and will be thoroughly examined in Section 2.

Further, despite the increasing attention given to the advantages of MPDs in published academic works, the industrial examples are still relatively limited, and the classical three-phase drives continue to dominate the motor drive industry due to their simplicity and cost-effectiveness. An example of an MPD that has been manufactured is the industrial drive DANA TM4 SUMO, a six-phase drive designed for heavy-duty EVs with a power range of 162 kW to 265 kW [16].

There are various types of AC electric machines available, but the primary types of machines that are typically used for electric vehicle traction applications are induction machines (IMs) and permanent magnet synchronous machines (PMSMs). The induction motor has been the workhorse in industrial drives because it is a well-known motor, it is cheap, and it does not require a position sensor to implement a low-cost control for low dynamic performance applications. The PMSM arises as a well-suited candidate to be used in automotive applications because of its high-power density. Unlike induction motors, there is no need to induce rotor currents to create the rotor magnetic field; thus, higher efficiency levels can be achieved. Moreover, PMSMs offer easy control strategies. An overview of the multiphase IM and PMSM topologies and the main theories to model them, such as vector space decomposition (VSD) [29,30] and the double *d-q* model [31], are covered in Section 3.

The general trend in power electronic devices is to switch the power semiconductors at increasingly higher frequencies in order to minimise harmonics and reduce passive component sizes. Nevertheless, increasing switching frequency increases the switching losses, which become especially significant at high power levels. One proposed method for decreasing the switching losses is to construct a converter with a high number of switching states and a low switching frequency, such as in the case of multilevel converters [32]. Multilevel converters are a type of architecture that improves the quality of the output voltage waveform, reduces dv/dt, and allows the creation of a high-power converter without the issue of switching series-connected semiconductor devices. Commonly used multilevel converters are the neutral point clamp (NPC), the flying capacitor (FC), and the various cascaded bridge converter topologies (CB). Multilevel converters are already commercially available, with the Converteam MV7000 and the Alstom Alspa VDM 6000 [33–36] as examples. Another developmental trend followed by researchers while designing power converters is to reduce the number of passive and active components to lower the overall costs of the converters and attain higher reliability.

In order to increase the power density of power electronics converters, one possible solution is to reduce the size of converters by using topologies that have a lower number of switches. The open-end winding topology (OEW), initially described in [33], can be considered an alternative method for generating multilevel phase voltage waveforms. The OEW drives have a reduced component count compared to traditional NPC and FC converters that are equivalent in function [13,37]. However, one disadvantage of this topology is that it requires two isolated DC power supplies to feed the inverters in order to prevent the flow of zero-sequence current. Another disadvantage is that the switches in the higher-voltage dc-link must be able to withstand twice the voltage of those in the equivalent NPC or FC. This review paper covers recent advancements from a topological perspective, and the most common topologies used for five-phase drive and six-phase drive

are presented in Sections 4 and 5, respectively. Further, more drive topologies that are less popular than five- and six-phase are addressed in Section 6.

The classical control and modulation techniques used to achieve the best performance in MPDs are covered in Section 7.

Section 8 discusses the current status, trends, and challenges in research on improving and incorporating MPDs in the EV industry. Finally, conclusions and future perspectives are provided in Section 9. Figure 1 illustrates the structure of the MPD review paper.

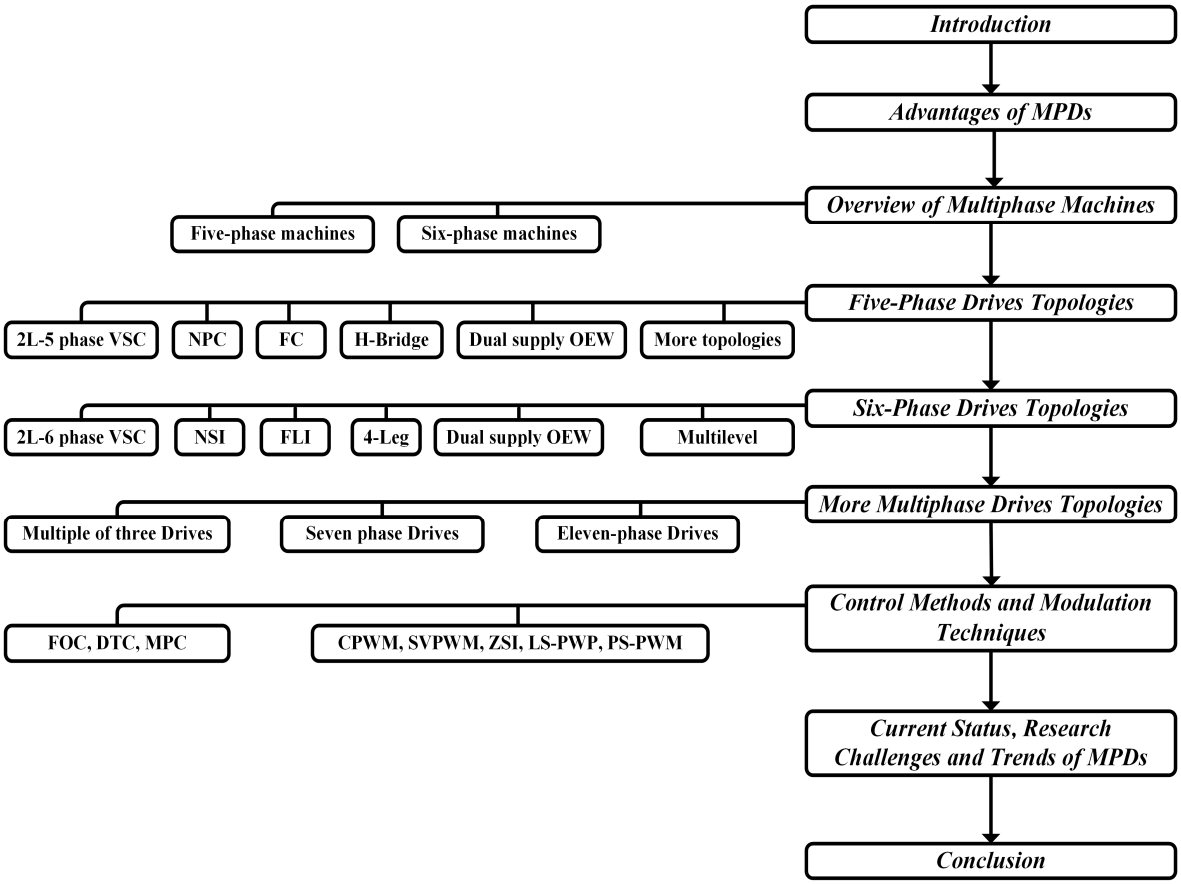

Figure 1. Schematic diagram illustrating different sections of the review paper on MPDs.

2. Advantages of Multiphase Drives

As mentioned in the introduction, there has been an upsurge of interest in multiphase machines (machines with more than three-phases). The reason is that multiphase drives are characterised by outstanding features compared to conventional three phase drives. In this section, some of these characteristics are highlighted.

2.1. Lower Power Rating per Phase

In multiphase drives, the power is distributed across a larger number of phases, and each phase is supplied by a converter leg. The power of an electric machine can be expressed as follows:

$$P = qV_{rms}I_{rms}\cos(\phi) \quad (1)$$

where q is the number of phases, I_{rms} is the root mean square (RMS) value of the phase current, V_{rms} is the root mean square value of the phase voltage, and $\cos(\phi)$ is the machine power factor. Using (1) for a constant power rating leads to the current p.u. graphs shown in Figure 2.

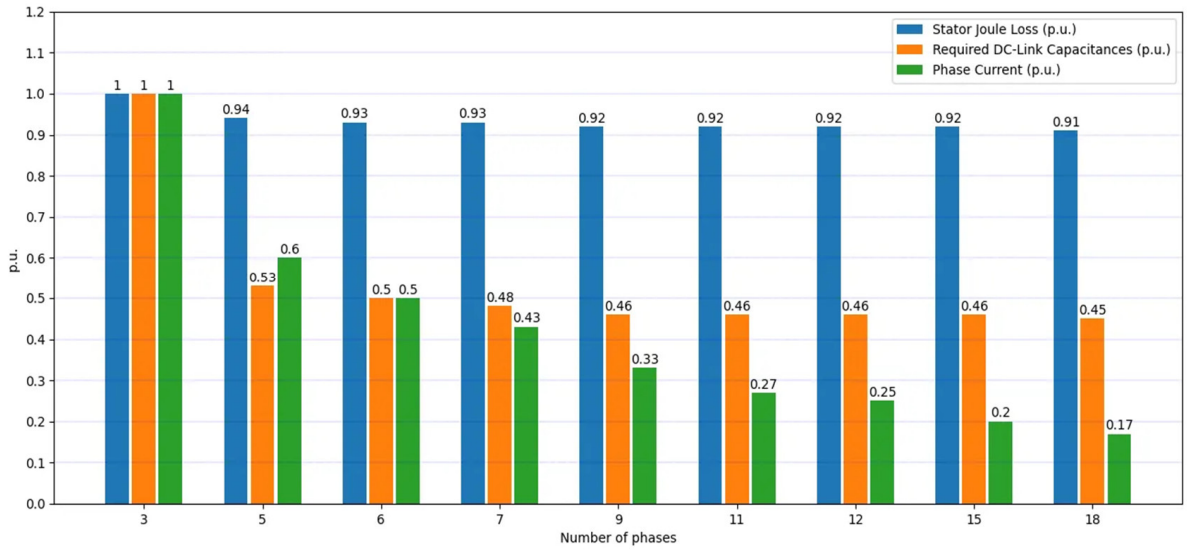

Figure 2. Joule loss, phase current, and required dc-link capacitance in p.u. for different numbers of phases, assuming constant power.

The relation between the number of phases and the per-phase current is inversely proportional. As the number of phases increases, the reduction in per-phase current becomes smaller. The phase currents of six-phase machines are half those of three-phase machines, meaning that the same power modules used for existing three-phase drives can be used and controlled separately to control different phases instead of being connected in parallel to control the same phase.

2.2. Better Fault Tolerance

The higher number of phases gives more flexibility under fault conditions. This feature makes MPDs excellent candidates for aerospace drives and electric vehicle applications. In faulty operation, the drive can operate continuously during a failure that occurs in the motor or inverter until the next maintenance, although at a lower power rating for the same phase current. The performance of the faulty drive can be enhanced using an optimization algorithm based on a specific performance criterion.

Among the different types of faults, the open-phase fault is the most common and the most studied faulty condition of an electric machine. An open-phase fault means one or more phases are lost because of a failure in the machine windings, control circuit, or power electronics, resulting in the phase(s) being considered an open circuit. One of the strategies for fault-tolerant control (FTC) that allows the operation of a drive even with the complete loss of one leg of the inverter or motor phase is proposed in [28]. The method uses a current–source inverter, and no hardware reconfiguration is needed. The approach is based on regulating the amplitudes and phases of the currents of the remaining phases to ensure the same rotating magnetic field as in healthy mode conditions. In addition, although there is no need for extra hardware, this fault tolerance is achieved by using an algorithm to detect this fault, as investigated in [38] for a six-phase induction machine. The FTC of multiphase machines does not only consist of redefining the current reference but also optimizing it to minimise losses or maximize the torque, as discussed in [26].

In more than one phase open-circuit fault, a specific analysis of the fault-tolerant capability of the six-phase induction machines has been investigated in [24]. The reference [23] proposed an improved approach for multiphase machines that effectively reduces stator losses over the entire range of torque operations in the case of a single open-circuit fault. Further, because the inverters losses that occur in faulty cases represent an essential part of the overall system efficiency, they should also be considered in the analysis by using different optimization criteria as described in [39,40].

2.3. Torque Density Improvement

The Improvement of torque density is an attractive aspect of MPDs that allows the creation of high-power density motor drives for EV applications. The current harmonic injection technique is used to enhance the torque density and reduce ripples.

The harmonic injection method is a technique that increases the torque density of motors by reshaping the flux distribution within the machine and thus obtaining higher fundamental flux densities. Basically, any current frequency can be injected into the machine, but the 3rd, 5th, and 7th are mostly used because of their significant amplitude.

The use of third harmonic injection in six-phase drives presents two challenges. The first issue is providing a neutral path for the currents to flow through. This problem is addressed in [41], and the suggested approach is to connect the neutral point of the machine winding to the midpoint of the dc-link with an additional proportional controller to balance the midpoint voltage at a stable level. This helps prevent the midpoint voltage from drifting during loading [42]. The other problem is optimising the flux pattern in the machine's air gap. When the machine is under load, the angle of the third harmonic current may change, leading to an uneven distribution of the resulting total air gap MMF. Several studies have addressed this issue [43,44]. The proposed solutions are based on artificial intelligence techniques such as genetic algorithms [43] and neural networks [44].

The optimal third harmonic amplitude that should be injected into the current for a dual three-phase machine is addressed in [45]. The amplitude depends on the ratio of the third harmonic back-EMF to the fundamental back-EMF.

Another proposal of current injection into the machine is explored in [46], which involves injecting fifth- and seventh-order harmonic currents in order to create a more flat top current waveform and increase the torque per fundamental current ampere. The only drawback, these harmonic currents are considered circulating currents that do not contribute to torque production. The optimization of the injected currents and efficiency analysis have been conducted in [47]. The use of these techniques can improve the torque per fundamental current ampere and significantly reduce the size and weight of the motor drives, addressing a key challenge in the field of electrified transportation research.

Figure 2 provides a summary of some of the features mentioned in the previous sections. Figure 2 illustrates the decrease in per-unit phase current, required dc-link capacitance [48], and reduction in stator joule loss [21] of several multiphase machines, namely five, six, seven, nine, eleven, twelve, fifteen, and eighteen-phase machines.

As shown in Figure 2, the improvement in stator losses and required dc-link capacitance will be less significant by increasing the number of phases. However, the modelling, control, and manufacturing will be more complicated and challenging. These disadvantages are the main reason for limiting the use of multiphase machines instead of conventional three-phase machines.

3. Multiphase Machines

This section will cover the topology of five-phase and six-phase machines. Moreover, the mathematical modelling of multiphase machines using *d-q* and vector space decomposition (VSD) is presented in this section.

3.1. Five-Phase Machines

The first five-phase motor was introduced in 1969, and a five-phase voltage–source inverter-fed induction motor was proposed [2]. The stator winding of a five-phase machine is illustrated in Figure 3, where the angle between two adjusted phases equals 72°.

A comparison of operating curves of five-phase and three-phase induction machines of the same size is presented in [49], and a comparative analysis based on finite element analysis of three-phase and five-phase PMSM is presented in [50]. The general conclusion of the comparison is that the five-phase machines produce higher electromagnetic torque and back-emf and lower cogging torque when compared to the three-phase machines.

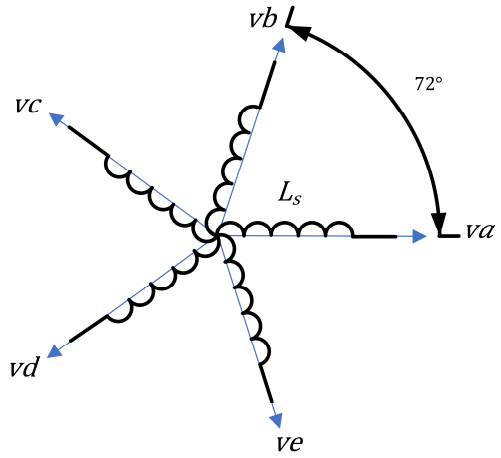

Figure 3. Five-phase stator winding for star connection.

3.2. Six-Phase Machines

The six-phase machines have benefits over their three-phase counterparts, regardless of machine topology (PMSMs or induction machines). A comparative study between both machines shows the advantages of the six-phase machines in terms of copper losses as well as space harmonic patterns [51]. The six-phase system demonstrates improved performance in terms of the air gap flux space harmonics of the 5th and 7th harmonics [51].

The efficiency analysis and comparison of pulse width modulation (PWM) inverter-fed three-phase and six-phase induction machines performed at the same dc-bus voltage are addressed in [52]. The experimental results have shown that the efficiency is almost the same, with a small error due to measured/simulated data uncertainties. The efficiency is not a discriminator in evaluating the performances and the advantages/disadvantages of three-phase and six-phase induction motor drives fed by PWM VSI. The advantages could be expected with the six-phase machine in situations where the copper losses are more significant than the iron losses, such as in low-frequency applications [53].

The six-phase machines have different winding configurations and different neutral connections. This section will cover the difference between common single neutral and two neutral connections and the different winding configurations of a six-phase machine.

3.2.1. Single Neutral and Two Neutral Configurations

There are two options for the connection of the stator phase winding, which depend on the connection of the neutral point. These options are a single neutral connection or two isolated neutral connections, as shown in Figure 4.

Figure 4. (**a**) Two neutral connections; (**b**) A single neutral connection for six-phase machine winding.

In [24], it has been shown that the connection of neutral points on the armature winding significantly affects the post-fault torque that the machine could generate under faulty conditions. Moreover, the single neutral connection leads to higher torque and provides

better fault-tolerant capability compared to two isolated neutral connections. In addition, the two isolated neutral connections cannot support the scenario of three open-circuit faults, and there is no possible postfault operation under this condition.

The single neutral point connection has been shown to be effective in maintaining fault-tolerant operation. In contrast, the two isolated neutral point connections have improved the utilisation of dc-link and simpler current controllers due to the inability for zero-sequence currents to physically flow in this type of connection.

However, a study has been proposed in [54] to take advantage of both configurations, isolated neutrals of connected neutrals, in terms of higher torque production and maximum speed. In the study, simple hardware and software modifications have been proposed to modify the neutral point configuration, as well as offline optimization schemes capable of identifying the optimization parameters throughout the entire torque-speed range, and this for different neutral point configurations.

3.2.2. Symmetrical, Asymmetrical, and Dual Six-Phase Machines

The six-phase machines have different winding configurations that vary based on the spatial angle between the two sets of three-phase windings. The machines with a 60° angle between their two sets of three-phase windings are referred to as symmetrical six-phase machines, while those with a space angle of 30° are classified as asymmetrical. The six-phase machine with no space angle difference between its two sets of three-phase windings is referred to as the dual three-phase machine (also known in some literature as a double-stator) [24]. The different configurations are shown in Figure 5.

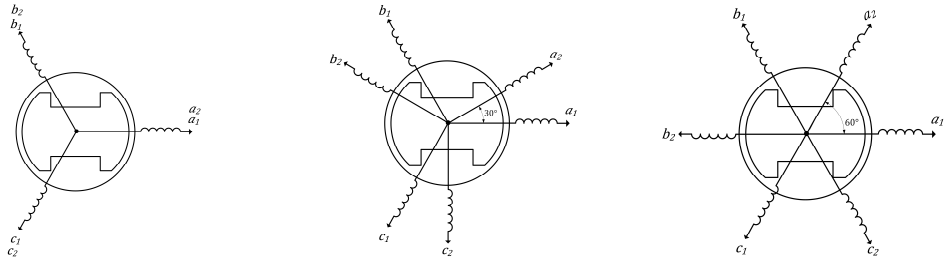

Figure 5. (**a**) Dual three-phase machine; (**b**) asymmetrical six-phase machine; (**c**) symmetrical six-phase machine.

The three mainstream six-phase machines (asymmetrical, symmetrical, and dual three-phase) are compared for their normal and faulty condition capability in [24], and a guideline for the selection of the most suitable six-phase machine for each specific application is illustrated in Table 1.

Table 1. Guidelines for the selection of the most suitable six-phase machine for each specific requirement.

Configuration	Asymmetrical	Symmetrical	Dual Three-Phase
Fault tolerance point of view of single open circuit fault	Best in 2N	Best in 1N	Worst
Fault tolerance point of view of two open circuit fault	All similar in 2N	All similar in 2N	All similar in 2N
	Best in 1N	Good in 1N	-
Fault tolerance point of view of three open circuit fault	Best in 2N in term of e fault-tolerant capability	Best in 1N	Best in 2N in term of simplicity and better dc-bus utilization. Worst in 1N
Torque range under faulty condition	-	Best	-
Torque under healthy condition	Lower torque ripple when operated with six-step inverter	Similar to asymmetrical with the modern high-frequency pulse-width modulation method	Similar to asymmetrical with the modern high-frequency pulse-width modulation method

In conclusion, a symmetrical machine is globally the machine with a higher post-fault capability in 1N configuration. The asymmetrical performance is quite similar to symmetrical, which keeps it competitive in terms of post-fault tolerance in 1N. The asymmetrical is the best choice in 2N. Even though dual three-phase has better performance than symmetrical and asymmetrical for some specific and limited scenarios, it is still the worst choice in terms of fault tolerance.

3.3. Mathematical Modelling of Multiphase Machines and Reference Theorey

The mathematical model of a multiphase machine is required to provide high-performance modulation and control techniques for MPDs. The vector space decomposition (VSD) is the foremost approach used to model multiphase machines, whatever the phase number. In machines with a multiple of three phases, another approach called "dual three-phase" (DTP) can be adopted.

The three-phase machines are usually modelled in the *Park* or *Clarke/Concordia* (amplitude invariant/power invariant) transformation. The three-phase equations in the "*ABC*" frame are reduced to only two equations in the rotating *d-q* or stationary *α-β* reference frame. The dual three-phase approach (DTP) uses the same methodology and models each three-phase set of multiphase machines separately.

The different modelling techniques and general mathematical equations applied to different multiphase machines are reviewed in this section, with special attention paid to the six-phase machine.

3.3.1. Coupled Double D-Q Transformation

The machines with multiple three-phase windings, such as 6-phase and 9-phase machines, are most frequently discussed among the multiphase machines. The use of multiple three-phase windings allows the use of well-established three-phase mathematical formulations. In the literature, particular attention has been given to the asymmetrical six-phase machines, where the machine can be driven using a six-phase voltage source inverter (VSI) or two separate three-phase VSIs and controlled in two individual *d-q* reference frames (or two individual *α-β* reference frames) simultaneously [55].

The winding reference frame configuration for a six-phase machine is illustrated in Figure 6.

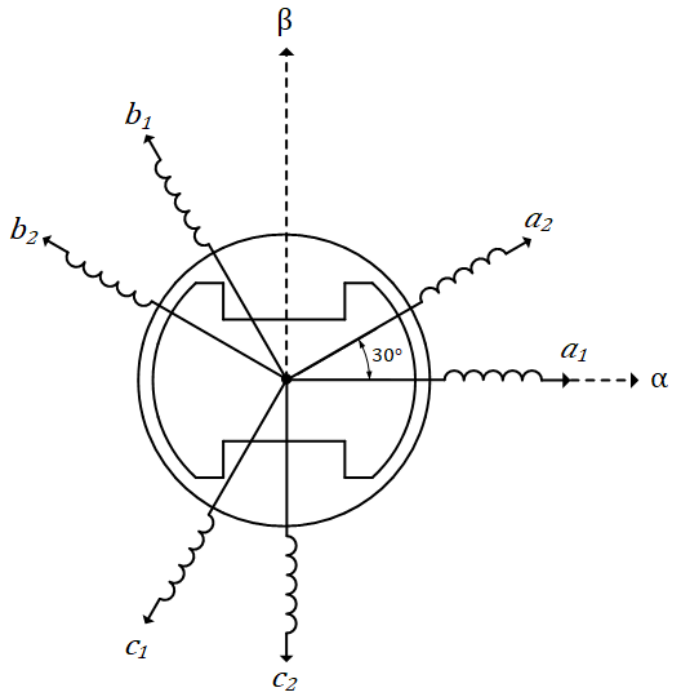

Figure 6. Reference configuration for coupled transformations.

For the stationary reference frame α-β, in the case that the α-axis is aligned with phase a_1 of stator winding, the two sets of *Clarke/Concordia* transformation, donated $\alpha_1 - \beta_1$ and $\alpha_2 - \beta_2$ components, are expressed as follows:

$$\begin{bmatrix} X_{a1} & X_{\beta 1} \end{bmatrix}^T = [T_1] \cdot \begin{bmatrix} X_{a1} & X_{b1} & X_{c1} \end{bmatrix}^T \tag{2}$$

$$\begin{bmatrix} X_{a2} & X_{\beta 2} \end{bmatrix}^T = [T_2] \cdot \begin{bmatrix} X_{a2} & X_{b2} & X_{c2} \end{bmatrix}^T \tag{3}$$

where X is a general symbol that can be voltage, current, or flux.

For the asymmetric machines with a spatial displacement of two sets of winding equal to 30°, the *Clarke* matrices T_1 and T_2 are given by:

$$[T_1] = k \begin{bmatrix} 1 & -\frac{1}{2} & -\frac{1}{2} \\ 0 & \frac{\sqrt{3}}{2} & -\frac{\sqrt{3}}{2} \end{bmatrix} \tag{4}$$

$$[T_2] = k \begin{bmatrix} \frac{\sqrt{3}}{2} & -\frac{\sqrt{3}}{2} & 0 \\ \frac{1}{2} & \frac{1}{2} & -1 \end{bmatrix} \tag{5}$$

where k is a coefficient equal to $\sqrt{\frac{2}{3}}$ and $\frac{2}{3}$ for the power invariant and magnitude invariant transformations, respectively.

The two sets of rotating park transformation components, donated $d_1 - q_1$ and $d_2 - q_2$, are expressed as follows:

$$\begin{bmatrix} X_{d1} & X_{q1} & X_{d2} & X_{q2} \end{bmatrix}^T = [P] \begin{bmatrix} X_{a1} & X_{b1} & X_{c1} & X_{a2} & X_{b2} & X_{c2} \end{bmatrix}^T \tag{6}$$

where X is a general symbol that can be voltage, current, or flux, and the matrix P is expressed as follows:

$$P(\theta) = k \begin{bmatrix} P_{1(\theta)} & 0_{3,3} \\ 0_{3,3} & P_{2(\theta)} \end{bmatrix} \tag{7}$$

$$[P_1] = k \begin{bmatrix} \cos\theta & \cos\left(\theta - \frac{2\pi}{3}\right) & \cos\left(\theta + \frac{2\pi}{3}\right) \\ -\sin\theta & -\sin\left(\theta - \frac{2\pi}{3}\right) & -\sin\left(\theta + \frac{2\pi}{3}\right) \end{bmatrix} \tag{8}$$

$$[P_2] = P_1\left(\theta - \frac{\pi}{6}\right) = k \begin{bmatrix} \cos\left(\theta - \frac{\pi}{6}\right) & \cos\left(\theta - \frac{2\pi}{3} - \frac{\pi}{6}\right) & \cos\left(\theta + \frac{2\pi}{3} - \frac{\pi}{6}\right) \\ -\sin\left(\theta - \frac{\pi}{6}\right) & -\sin\left(\theta - \frac{2\pi}{3} - \frac{\pi}{6}\right) & -\sin\left(\theta + \frac{2\pi}{3} - \frac{\pi}{6}\right) \end{bmatrix} \tag{9}$$

where θ is the angular position of the rotor d-axis with respect to the axis of phase a_1.

By applying the *Park* transformation to the inductance matrix and assuming that the winding sets are identical ($L_{d1} = L_{d2} = L_d$, $L_{q1} = L_{q2} = L_q$, $M_{d12} = M_{d21} = M_d$, $M_{q12} = M_{q21} = M_q$), the d-q frame inductance matrix, L_{T1}, with dimension 4×4 can be expressed as:

$$L_{T1} = \begin{bmatrix} L_{dq} & M_{dq} \\ M_{dq} & L_{dq} \end{bmatrix} \tag{10}$$

$$L_{dq} = L_{dq} = \begin{pmatrix} L_d & 0 \\ 0 & L_q \end{pmatrix} \tag{11}$$

$$M_{dq} = \begin{pmatrix} M_d & 0 \\ 0 & M_q \end{pmatrix} \tag{12}$$

where L_{dq} and M_{dq} are the self and mutual inductance matrices, respectively.

The flux equation is given by:

$$\begin{bmatrix} \psi_{d1} \\ \psi_{q1} \\ \psi_{d2} \\ \psi_{q2} \end{bmatrix} = \begin{bmatrix} L_d & 0 & M_d & 0 \\ 0 & L_q & 0 & M_q \\ M_d & 0 & L_d & 0 \\ 0 & M_q & 0 & L_q \end{bmatrix} \begin{bmatrix} i_{d1} \\ i_{q1} \\ i_{d2} \\ i_{q2} \end{bmatrix} + \begin{bmatrix} \psi_{\mathrm{PM},d1} \\ 0 \\ \psi_{\mathrm{PM},d2} \\ 0 \end{bmatrix} \tag{13}$$

where the subscript "d_1" refers to the d-axis component of the first winding set and "q_2" to the q-axis component of the second winding set.

The matrix form (10) illustrates the structure of the inductance matrix in the *d-q* frame. The inductance matrix is not diagonal, and the off-diagonal mutual inductance terms in the matrix describe the magnetic coupling between the two different winding sets, which is the main reason why six-phase machines are more difficult to control and model than conventional three-phase machines.

The set of Equation (13) describes a multiple-input, multiple-output system with a coupling between them. However, a typical PI-controller-based current control configuration works better if such coupling does not exist [55].

In order to eliminate the coupling, new voltage terms can be expressed as follows [55]:

$$\begin{aligned} \left| v_{d1}^{\text{decoupling}} \right. &= M_d \tfrac{di_{d2}}{dt} - \omega L_q i_{q1} - \omega M_q i_{q2} \\ \left| v_{q1}^{\text{decoupling}} \right. &= M_q \tfrac{di_{q2}}{dt} + \omega L_d i_{d1} + \omega M_d i_{d2} + \omega \psi_{\text{PM},d1} \\ \left| v_{d2}^{\text{decoupling}} \right. &= M_d \tfrac{di_{d1}}{dt} - \omega L_q i_{q2} - \omega M_q i_{q1} \\ \left| v_{q2}^{\text{decoupling}} \right. &= M_q \tfrac{di_{q1}}{dt} + \omega L_d i_{d2} + \omega M_d i_{d1} + \omega \psi_{\text{PM},d2} \end{aligned} \tag{14}$$

where ω is the electrical speed of the machine.

The elimination of all the cross-coupling effects between the voltage equations would require feeding the following decoupling terms presented in (14) as positive feedback to the output of the current controllers. In this case, the control strategy is called feedforward decoupling control.

However, without any decoupling feedback, neglecting the cross-coupling between two sets may not affect the zero steady-state error much in terms of current tracking [55]. Further, the magnetic coupling between the winding sets strongly affects the dynamic performance of the machine, and by neglecting it, the torque will not be estimated correctly, especially if the machine has saliency $(L_d \neq L_q)$ [55].

3.3.2. Decoupled Double D-Q Transformation

In order to eliminate the equation's magnetic coupling without the use of the feedforward decoupling control, the decoupled double *d-q* model is developed. The decoupled *Park* transformation will be noted in this paper as $[P^*]$. In eliminating such coupling and diagonalizing the inductance matrix L_{T1}, a decoupling matrix is used as [56]:

$$\boldsymbol{T}_{dec} = k' \begin{pmatrix} 1 & 0 & 1 & 0 \\ 0 & 1 & 0 & 1 \\ 0 & 1 & 0 & -1 \\ -1 & 0 & 1 & 0 \end{pmatrix} \tag{15}$$

where k' is the orthonormalization coefficient equal to $\frac{1}{\sqrt{2}}$ and $\frac{1}{2}$ for the power invariant and magnitude invariant transformations, respectively.

Applying (15) to (10), we get the diagonal inductance L_{T2}:

$$\boldsymbol{L}_{T2} = \boldsymbol{T}_{dec} \boldsymbol{L}_{T2} \boldsymbol{T}_{dec}^{\mathrm{T}} = \begin{pmatrix} L_{D_1^*} & 0 & 0 & 0 \\ 0 & L_{Q1^*} & 0 & 0 \\ 0 & 0 & L_{D2^*} & 0 \\ 0 & 0 & 0 & L_{Q2^*} \end{pmatrix} \tag{16}$$

where the decoupled inductances are defined by:

$$\begin{vmatrix} L_{D_1^*} = L_d + M_d \\ L_{Q_1^*} = L_q + M_q \\ L_{D_2^*} = L_q - M_q \\ L_{Q_2^*} = L_d - M_d \end{vmatrix} \tag{17}$$

and the decoupled *Park* matrix, P^*, which is obtained by multiplying (15) by (8) as follows:

$$P^*(\theta) = k' \begin{bmatrix} P_{1(\theta)} & P_{1(\theta-\frac{\pi}{6})} \\ P_{1(\theta+\frac{\pi}{2})} & P_{1(\theta-\frac{\pi}{6}-\frac{\pi}{2})} \end{bmatrix} \tag{18}$$

where P_1 is the matrix presented in (8).

It is important to note that the proposed transformation eliminates third harmonics and their multipliers from the transformed variables.

Additionally, it is crucial to note that the voltage, current, and flux parameters in the *d-q* reference using decoupled transformation are not the same as using coupled transformation. Therefore, it is desirable to provide a better physical interpretation of the model variables by relating them to variables in the coupled double *d-q* model. The relations between both transformations in the case of power invariants are formulated below:

$$\begin{bmatrix} X_{d1}^* & X_{q1}^* & X_{d2}^* & X_{q2}^* \end{bmatrix}^T = [P^*] \begin{bmatrix} X_{a1} & X_{b1} & X_{c1} & X_{a2} & X_{b2} & X_{c2} \end{bmatrix}^T \tag{19}$$

$$\begin{vmatrix} X_{d1}^* = \sqrt{\frac{1}{2}}(X_{d1} + X_{d2}) = \sqrt{\frac{1}{2}}\Sigma X_d \\ X_{q1}^* = \sqrt{\frac{1}{2}}(X_{q1} + X_{q2}) = \sqrt{\frac{1}{2}}\Sigma X_q \\ X_{d2}^* = \sqrt{\frac{1}{2}}(X_{q1} - X_{q2}) = \sqrt{\frac{1}{2}}\Delta X_q \\ X_{q2}^* = \sqrt{\frac{1}{2}}(-X_{d1} + X_{d2}) = -\sqrt{\frac{1}{2}}\Delta X_d \end{vmatrix} \tag{20}$$

where X is a general symbol that can be voltage, current, or flux.

In the previous formulation, the electrical angle θ is the angle between the d-axis and "a_1"phase. However, another interesting electromagnetic configuration is illustrated in Figure 7 and presented in [56]. As shown in Figure 7, the angle θ is between the d-axis and the middle angle of "a_1" and "a_2" with the angle displacement α equal to $\frac{\pi}{12}$.

The equation of decoupled *Park* transformation formulated in (18) is modified to the following equation for power invariant transformation:

$$P_2^*(\theta) = \frac{1}{\sqrt{2}} \begin{bmatrix} P_{1(\theta+\alpha)} & P_{1(\theta-\alpha)} \\ P_{1(\theta+\alpha+\frac{\pi}{2})} & P_{1(\theta-\alpha-\frac{\pi}{2})} \end{bmatrix} \tag{21}$$

where P_1 is the matrix presented in (8).

This special configuration yields decoupled *d-q* reference frames with similar properties as the *d-q* and *z1-z2* subspaces of the vector space decomposition (VSD), which will be discussed in detail in the next section.

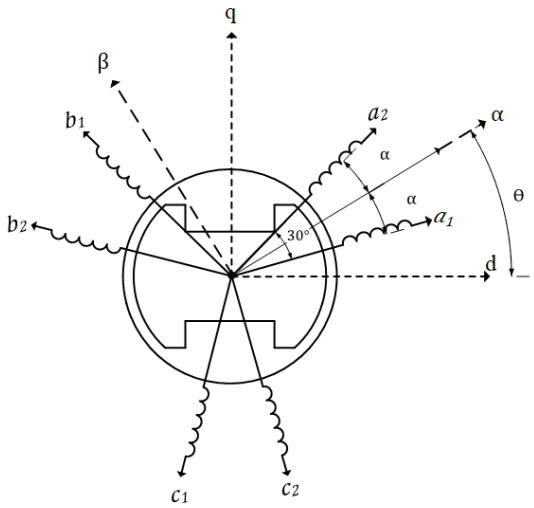

Figure 7. Reference frame configuration for decoupled transformation.

3.3.3. Vector Space Decomposition (VSD)

While the double *d*-*q* transformation (or α-β for stationary transformation) can only be applied in the case multiple of three-phase machines, the vector space decomposition provides an alternative approach that can be applied for multiphase machines with any number of phases, including the multiple three-phase machines. This approach is presented in different literature [21,29,31].

In using vector space decomposition (VSD), the analytical modelling and control of the *n*-phase electric machine are accomplished in $\frac{n}{2}$ orthogonal subspaces (or $\frac{n-1}{2}$ for a machine with an odd number of phases). The orthogonal subspaces include only one α-β subspace and several *x*-*y* subspaces and zero sequence components. The dynamics of the electromechanical energy conversion related and non-electromechanical energy conversion related machine variables are thereby totally decoupled, which facilitates machine control and modelling [29]. In other words, the parameters that create useful power and the ones that do not are decoupled. In a machine with sinusoidal magnetomotive force distribution, the α-β components contribute to useful electromechanical energy conversion, while the *x*-*y* and zero-sequence components only produce losses [31]. Further, in odd phase numbers, zero-sequence components do not exist in any star-connected multiphase system without a neutral conductor (an isolated neutral point), as the zero-sequence currents cannot flow. On the other hand, zero components can exist if the phase number is even.

The VSD transformation has the ability to separate the harmonics and map them into each subspace. The VSD transformation has the properties listed below [29]:

- The fundamental components of the machine variables (voltage, current, and flux) and the kth harmonics with $k = 12m \pm 1$, $(m = 1, 2, 3, \ldots)$ are transformed into the *d*-*q* subspace. It should be pointed out that the d-q axes have been chosen in such a manner that they coincide with the plane of rotation of the air gap flux. Therefore, these variables will produce a rotating MMF in the machine airgap and thus be related to electromechanical energy conversion.
- The harmonics with $k = 6m \pm 1$, $(m = 1, 3, 5, \ldots)$ harmonics, are mapped into the *z1*-*z2* subspace. The variables on this plane will not generate any rotating MMF in the airgap and thus be non-electromechanical energy related as the *z1*-*z2* subspace is orthogonal to the *d*-*q* subspace.
- The zero sequence components with $k = 3m$, $(m = 1, 2, 3, \ldots)$ harmonics are mapped into the o_1-o_2 subspace to form the conventional zero sequence components.

The following discussion is addressed to the general formulation for multiphase machines. For an odd or even *n*-phase symmetrical machines the special displacement between two consecutive phases is equal to $\frac{2\pi}{n}$.

In assuming that the windings are sinusoidally distributed and the windings are star connected with a single neutral point, the stationary $\alpha - \beta$ decoupling transformation matrix is given in power invariant form (*Concordia*) in (22) with the angle $\alpha = \frac{2\pi}{n}$.

The Equation (22) is applicable to synchronous and asynchronous machines:

$$C = \sqrt{\frac{2}{n}} \begin{bmatrix} 1 & \cos\alpha & \cos 2\alpha & \cos 3\alpha & \dots & \cos 3\alpha & \cos 2\alpha & \cos\alpha \\ 0 & \sin\alpha & \sin 2\alpha & \sin 3\alpha & \dots & -\sin 3\alpha & -\sin 2\alpha & -\sin\alpha \\ 1 & \cos 2\alpha & \cos 4\alpha & \cos 6\alpha & \dots & \cos 6\alpha & \cos 4\alpha & \cos 2\alpha \\ 0 & \sin 2\alpha & \sin 4\alpha & \sin 6\alpha & \dots & -\sin 6\alpha & -\sin 4\alpha & -\sin 2\alpha \\ 1 & \cos 3\alpha & \cos 6\alpha & \cos 9\alpha & \dots & \cos 9\alpha & \cos 6\alpha & \cos 3\alpha \\ 0 & \sin 3\alpha & \sin 6\alpha & \sin 9\alpha & \dots & -\sin 9\alpha & -\sin 6\alpha & -\sin 3\alpha \\ \dots & \dots & \dots & \dots & \dots & \dots & \dots & \dots \\ 1 & \cos\left(\frac{n-2}{2}\right)\alpha & \cos 2\left(\frac{n-2}{2}\right)\alpha & \cos 3\left(\frac{n-2}{2}\right)\alpha & \dots & \cos 3\left(\frac{n-2}{2}\right)\alpha & \cos 2\left(\frac{n-2}{2}\right)\alpha & \cos\left(\frac{n-2}{2}\right)\alpha \\ 0 & \sin\left(\frac{n-2}{2}\right)\alpha & \sin 2\left(\frac{n-2}{2}\right)\alpha & \sin 3\left(\frac{n-2}{2}\right)\alpha & \dots & -\sin 3\left(\frac{n-2}{2}\right)\alpha & -\sin 2\left(\frac{n-2}{2}\right)\alpha & -\sin\left(\frac{n-2}{2}\right)\alpha \\ \frac{1}{\sqrt{2}} & \frac{1}{\sqrt{2}} & \frac{1}{\sqrt{2}} & \frac{1}{\sqrt{2}} & \dots & \frac{1}{\sqrt{2}} & \frac{1}{\sqrt{2}} & \frac{1}{\sqrt{2}} \\ \frac{1}{\sqrt{2}} & -\frac{1}{\sqrt{2}} & \frac{1}{\sqrt{2}} & -\frac{1}{\sqrt{2}} & \dots & -\frac{1}{\sqrt{2}} & \frac{1}{\sqrt{2}} & -\frac{1}{\sqrt{2}} \end{bmatrix} \begin{matrix} \alpha \\ \beta \\ x_1 \\ y_1 \\ x_2 \\ y_2 \\ \dots \\ \frac{x_{n-4}}{2} \\ \frac{y_{n-4}}{2} \\ o_+ \\ o_- \end{matrix} \quad (22)$$

The first two rows of the matrix presented in (22) define variables that will contribute to fundamental flux and torque production in α-β subsystem. The last two rows of the transformation matrix in (22) define the two zero sequence components and can be disregarded for all odd phase numbers n.

In multiphase induction machines, since the rotor winding is short-circuited, neither x-y nor zero-sequence components can exist, and only α-β equations of the rotor winding need to be considered.

In assuming that the induction machine equations are transformed into an arbitrary frame of reference that rotates at an angular speed ω_e, the model of an n-phase induction machine with sinusoidal winding distribution can be expressed as [21]:

$$\begin{aligned} v_{ds} &= R_s i_{ds} - \omega_e \psi_{qs} + p\psi_{ds} \\ v_{qs} &= R_s i_{qs} + \omega_e \psi_{ds} + p\psi_{qs} \\ v_{x1s} &= R_s i_{x1s} + p\psi_{x1s} \\ v_{y1s} &= R_s i_{y1s} + p\psi_{ys} \\ v_{x2s} &= R_s i_{x2s} + p\psi_{x2s} \\ v_{y2s} &= R_s i_{y2s} + p\psi_{y2s} \\ &\dots \\ v_{o+s} &= R_s i_{o+s} + p\psi_{o+s} \\ v_{o-s} &= R_s i_{o-s} + p\psi_{o-s} \\ v_{o-s} &= R_s i_{o-s} + p\psi_{o-s} \\ v_{dr} &= 0 = R_r i_{dr} - (\omega_e - \omega)\psi_{qr} + p\psi_{dr} \\ v_{qr} &= 0 = R_r i_{qr} + (\omega_e - \omega)\psi_{dr} + p\psi_{qr} \end{aligned} \quad (23)$$

with

$$\begin{aligned} \psi_{ds} &= (L_{ls} + L_m) i_{ds} + L_m i_{dr} \\ \psi_{qs} &= (L_{ls} + L_m) i_{qs} + L_m i_{qr} \\ \psi_{x1s} &= L_{ls} i_{x1s} \\ \psi_{y1s} &= L_{ls} i_{y1s} \\ \psi_{x2s} &= L_{ls} i_{x2s} \\ \psi_{y2s} &= L_{ls} i_{y2s} \\ &\dots \\ \psi_{o+s} &= L_{ls} i_{o+s} \\ \psi_{o-s} &= L_{ls} i_{o-s} \\ \psi_{dr} &= (L_{lr} + L_m) i_{dr} + L_m i_{ds} \\ \psi_{qr} &= (L_{lr} + L_m) i_{qr} + L_m i_{qs} \end{aligned} \quad (24)$$

where the symbols R, L, p, V, I, and ψ stand for resistance, inductance, time derivative, voltage, current, and flux linkage, respectively.

As stator to rotor coupling takes place only in α-β equations, rotational transformation is applied only to these two pairs of equations. The form of this transformation is the same as for a three-phase machine.

It is observed that the stator equations in the x-y and the $o_1 - o_2$ subspaces have the same form and the same parameters, and this is due to the assumption that the stator mutual leakage inductances are ignored.

In terms of machine control, it is also important to note that the control of d-q currents is crucial for flux and torque regulation. However, the non-electromechanical energy conversion related variables, which are on the x-y and the $o_1 - o_2$ plane, are very important and should be controlled to be as small as possible to reduce the extra losses in the machine, reduce the machine/converter current asymmetry, and achieve dead-time effect compensation [31].

4. Drive topologies for five-phase machines

This section presents different topologies of the five-phase drives, starting from the classical two-level voltage source converter (VSC), characterised by low-power and low-voltage, to more complicated topologies, such as the multilevel converter. The three multilevel converter topologies could be considered classic multilevel topologies, such as NPC, FC, and CHB, and they are discussed in this section. Moreover, some less-known topologies are briefly covered.

4.1. Two-Level, Five-Phase VSC

The first recorded use of a five-phase motor drive dates back to 1969. A two-level, five-phase, inverter-fed induction motor drive (also called a 10-pulse inverter) was proposed in [2]. The two-level, five-phase VSC is a popular topic of study due to its relatively simple structure and control compared to more complex topologies, such as matrix and multilevel converters.

The two-level VSC is mainly used for the low-power, and low-voltage motor drive sector. There are two strategies that can be employed for high-power applications using this simple topology. Current converters in parallel have low voltage with high current, while those in series have high voltage and low current. The method of low voltage with parallel converters has been widely adopted in 3-phase high/medium voltage (HV/MV) applications and especially in wind turbine converters, where the series connection does not result in any reduction of dv/dt (the derivative of voltage) or improvements in power quality. Similarly, drives connected in parallel can be used for multiphase drives for high-power applications. The two-level VSC is shown in Figure 8.

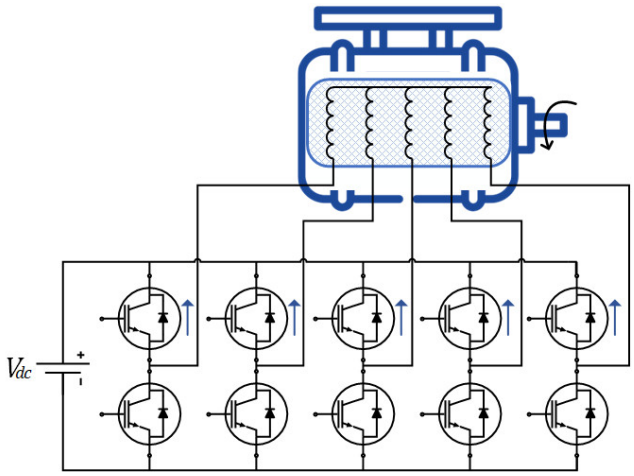

Figure 8. Two-level converter topology for a five-phase voltage source drive.

The two-level converters for five-phase drives offer some advantages, but there are still certain limitations that need to be considered, such as high THD and EMI, high voltage stress, high *dv/dt*, and the fact that they cannot be used for high voltage applications.

4.2. Multilevel Converters: Neutral Point Clamped Converters (NPC)

In power electronic devices, one solution to minimise harmonics and reduce passive component sizes is to increase the switching frequency. The increase in switching frequency increases the switching loss. For this reason, researchers have proposed a new drive topology in the form of multilevel converters, characterised by a high number of switching states. With more switching states, the inverter's output voltage can be stepped in smaller increments. This method allows for harmonic mitigation at low switching frequencies, thereby reducing switching losses. Moreover, this reduces electromagnetic compatibility (EMC) problems through the lower common-mode current facilitated by lower *dv/dt* produced by smaller voltage steps.

The two most known multilevel converters are the three-level neutral point clamped converter (3L-NPC) and the four-level neutral point clamped converter (4L-NPC). The earliest development of 3L-NPC and 4L-NPC was back in late 1970 using the diode clamped concept [57]. The work presented in [57] was further explored and improved, resulting in the development of the 3L-NPC as known today and later becoming the first multilevel converter to be implemented in industrial applications used for three-phase machine drives [58,59]. The 3L-NPC has gained popularity due to its simple power circuit structure compared to the 4L-NPC, with a lower power switch count and a lower number of capacitors [35].

The researchers have mainly considered the multilevel inverter with three-phase machines. However, the multilevel topology can be used for any machine phase number just by having the number of legs equal to the number of phases. The three-level neutral-point-clamped converters (3L-NPCs) for multiphase drives are covered in [60], which proposes a new modulation strategy without the use of linear controllers. The 3L-NPC for a five-phase machine using a novel optimal space vector modulation technique based on the switching state minimization method, which eliminates the undesired switching vectors and simplifies the vector space domain, is presented in [61].

Furthermore, another comparative performance of a five-phase, three-level neutral point clamped with a five-phase, two-level inverter for the same loading over a wide range of modulation index is studied in [62]. The experimental validation shows that the 3-level NPC VSI has better performance in terms of CMV and THD over a wide range of modulation indices.

The comparison in terms of voltage/current THD and implementation complexity of carrier-based PWM modulation strategies (CBPWMs) and space vector modulation strategies (SVPWMs) for a three-level, five-phase NPC converter is presented in [63]. The simulation and experimental results show that CBPWM techniques are simpler and require less computation time than their SVPWM counterparts. Therefore, they are better suited for multilevel, multiphase industrial applications. In the following, the topologies of the multiphase drives will be further discussed.

The 3L-NPC utilises an arrangement of four power switches per leg, connected through diodes to the midpoint of the dc-link, as illustrated in Figure 9. In this configuration, each switch blocks half of the total dc-link voltage.

The 4L-NPC uses an arrangement of three capacitor blocks and six power switches per leg, connected through diodes to the midpoint of the capacitor blocks, as illustrated in Figure 10.

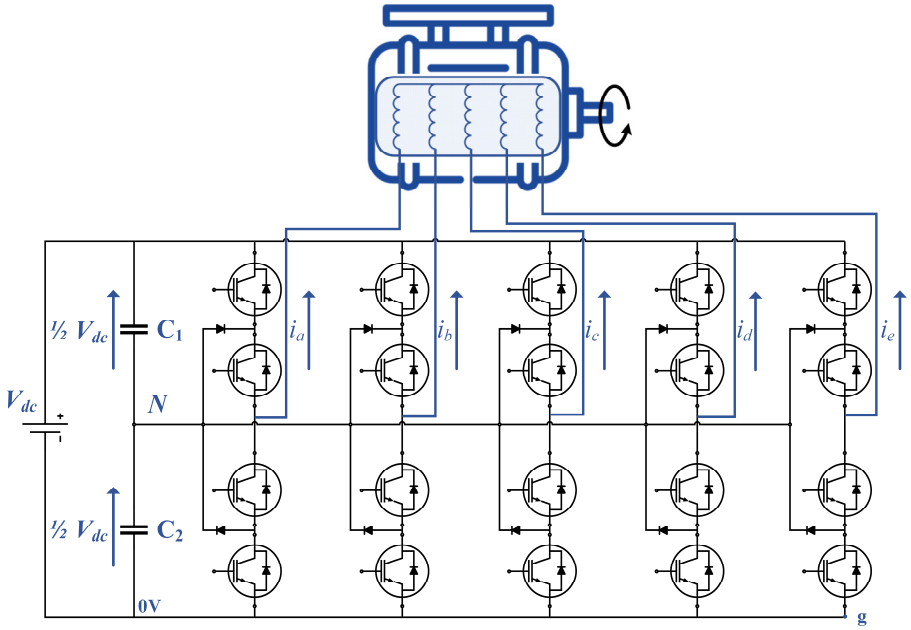

Figure 9. Three-level converter topology for a five-phase voltage source drive.

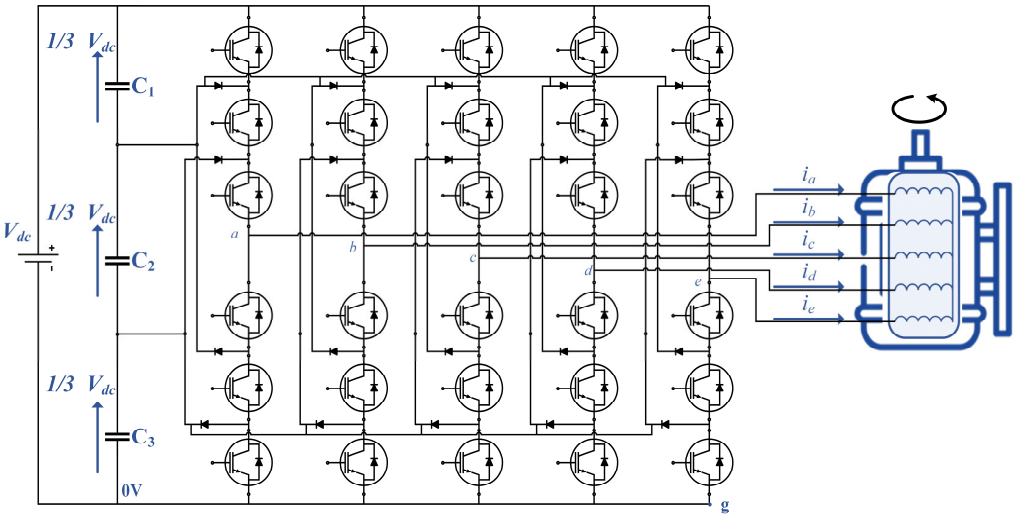

Figure 10. Four-level converter topology for a five-phase voltage source drive.

In general, for an n-level inverter, the phase-to-ground voltages can be expressed as [37]:

$$V_{xg} = \frac{k}{n-1} V_{dc} \qquad k = 0, 1, \ldots (n-1) \tag{25}$$

where "x" represents the phase, which can be "a", "b", "c", "d", or "e", and k represents the phase level selected by the gating signals as described above.

For example, in a three-level converter, as illustrated in Figure 9, the two dc capacitors split the dc rail voltage, allowing three different voltage levels to be selected. The phase voltage V_{ag} (phase a as an example) will be 0 if the two lower transistors in the a-phase are gated on, $^1/_2V_{dc}$ if the two centre transistors are gated on, and V_{dc} if the two upper transistors are gated on. Further, in the four-level converter, the phase to ground voltage levels are 0, $\frac{1}{3}V_{dc}$, $\frac{2}{3}V_{dc}$, V_{dc} selectable by gating on three switches per phase [64].

In referring to Figures 9 and 10, one can notice that the leg of n-level inverter is composed of $2(n-1)$ power switches, $(n-1)$ capacitors, $2(n-2)$ clamping diodes, and $(n-2)$ neutral midpoint between two capacitors.

In general, the number of possible switching states, N_{sw}, for a multilevel converter is given by [37]:

$$N_{sw} = n^p \tag{26}$$

where p is the number of phases. In a five-phase three-level converter, the number of possible switching states is $3^5 = 243$, and for a five-phase four-level converter, $4^5 = 1024$.

Despite all the advantages listed above, the 3L-NPC has a major disadvantage as the power switches do not have symmetric losses dissipation, forcing uneven heat distribution, which reduces the reliability of this popular topology [65]. Moreover, a voltage balancing of the dc-link capacitor is required [66]. In addition, this topology requires high speed clamping diodes that will be subject to reverse recovery stress.

In order to tackle the main drawback of the NPC, the neutral clamping diodes can be replaced by clamping switches to give a controllable path for the neutral current and control the loss distribution among the switches of the converter. This modified topology is called active NPC (ANPC), and it is illustrated in Figure 11 for the case of a 3-level ANPC. As explained before, ANPC allows for the neutral current to be controlled, enabling the losses to be evenly distributed among devices. Consequently, higher power ratings or higher switching frequencies can be achieved [67,68].

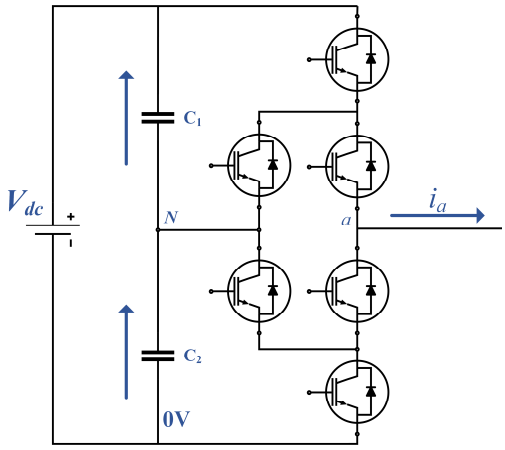

Figure 11. 3L-ANPC phase leg.

4.3. Multilevel Converters: Flying Capacitor (FC) Converters

The concept of a "light capacitor" (FC) has been around since the early 1970s [69]. The FC generates additional voltage levels, which reduces the voltage stress on the power switches by clamping a flying capacitor between two devices, as shown in Figure 12.

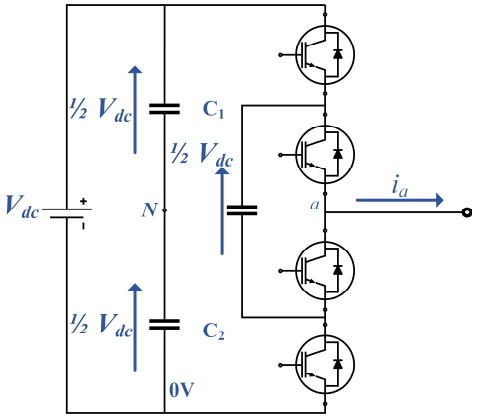

Figure 12. Three-level flying capacitor converter phase leg.

A pair of switches and one FC form a power cell. More cells can be connected, increasing the number of voltage levels of the converter. The FC can be controlled using FOC and by applying phase-shifted PWM (PS-PWM) for modulation [34,70], which ensures that the capacitor voltage is naturally balanced at the desired value.

The main limitations of this topology are the high switching frequencies required in order to balance FCs (whether a self-balancing or a control-assisted balancing modulation method is used). Moreover, the high number of capacitors reduces the system's reliability as they are more prone to failure than other components of the converter. This topology also requires the initialization of the FC voltages [34]. The FC converters can be used for MPDs.

4.4. Multilevel Converters: Cascaded H-Bridge Converter

The cascaded H-bridge converter topology for five-phase machines consists of five-phases of H-bridge power cells connected in series, as demonstrated in Figure 13 for the case of two cells per phase. The series connection increases the converter voltage and subsequently the power of the converter, with the ability to utilise low voltage power switches. The number of output voltage levels is $2k + 1$, where k is the number of cells.

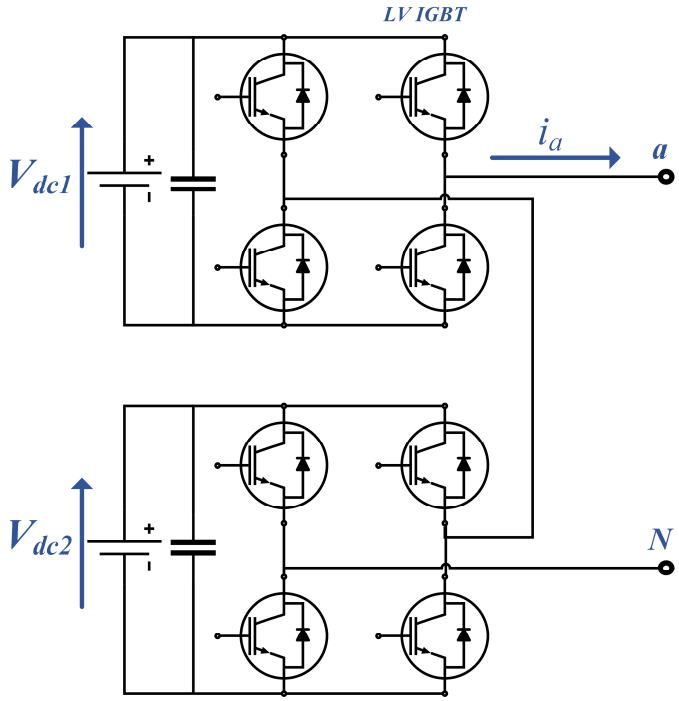

Figure 13. Two cells, a five-level cascaded H-bridge converter phase leg.

Due to the modularity of this topology, CHBs can have a high number of output voltage levels. For example, in the case of 8 cells, the CHBs can be found to have up to 17 levels or more with a low voltage source. This converter is typically controlled with FOC with phase-shifted PWM (PS-PWM) [34,70] and operates with low switching frequencies, resulting in reduced switching losses. Moreover, the output voltage harmonic content is shifted k (number of cells) times to higher frequencies, and due to the high number of output voltage levels, this converter does not typically require an output filter for most applications. In addition to its power quality, the CHB is well suited for high-power applications because of its modular structure, which enables higher voltage operation with classic low-voltage semiconductors [34].

The main drawback of this topology is the requirement for isolated dc sources to power each H-bridge. Additionally, due to its complex front end, it is uncommon to see this converter used in regenerative applications, especially since CHB needs a substan-

tially higher number of devices (two-level voltage source inverter per cell) to achieve a regenerative option. Further, CHB has a larger footprint compared to other topologies.

In comparison to the NPC topology, the NPC and CHB topologies generate the same number of levels when using the same number of power switches.

4.5. Five-Phase Dual Supply Open-End Winding Drives

The dual supply open-end winding topology is applied to machines with open winding topologies where access to two winding terminals is possible. This topology is based on feeding the five-phase winding via two isolated two-level VSIs, as shown in Figure 14. As illustrated, the VSI is fed from two isolated dc voltage sources, V_{dc1} and V_{dc2}.

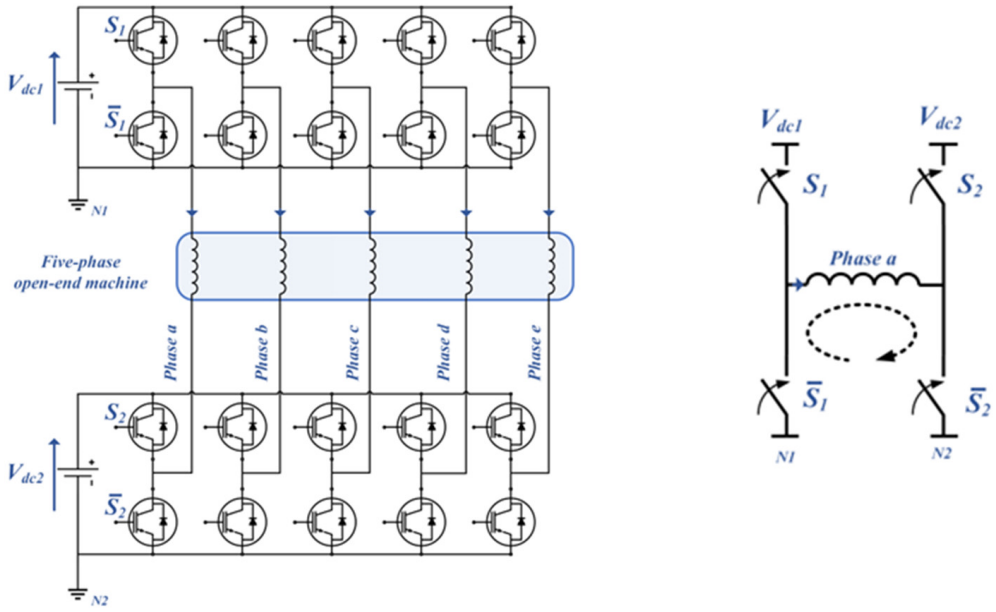

(**a**) (**b**)

Figure 14. (**a**) Five-phase dual supply drive; (**b**) Corresponding inverter leg.

The need for isolated dc-links is not an issue in EV applications, where the isolated supplies can be created using batteries. As the batteries are isolated dc sources, a capacitor voltage balancing technique is not required. Furthermore, in EV applications, the dc-source is a pack of batteries that can be rearranged to have various voltage levels and supply the drive. The merit of such topology is the possibility of using low dc-link voltage.

It has been shown in [37] that by changing the dc-source voltage ratios V_{dc1}/V_{dc2}, the voltage vector patterns (voltage levels) can be changed. The utilisation of two isolated two-level inverters with equal dc-link voltages allows for drive operation with a voltage waveform similar to that which can be obtained with a three-level voltage-source inverter in the single-sided supply mode [37]. Moreover, in the case where $V_{dc2} = 0$, the voltage vector plot is the same as that of a two-level converter, and with $V_{dc2} = \frac{V_{dc1}}{2}$, the pattern is the same as that of a four-level converter.

In [71], the OEW four-level five-phase drive is introduced, where the drive consists of a five-phase induction machine with open-end stator windings that are powered by two-level voltage source inverters with isolated dc-link voltages in a 2 : 1 ratio. This topology has demonstrated potential for use in EV/HEV applications where the dc-link voltages are low and the isolation of the supplies is more easily attainable. The benefits and drawbacks of using the four-level OEW drive will vary based on EV/HEV-specific configurations, for example, the dc-dc converter structure, battery packs, and charging topology, and will need to be evaluated on a case-by-case basis. A comparison of the aforementioned converter topologies is presented in Table 2.

Table 2. Comparison between different converter topologies for five-phase drives.

	Conventional 2-Level	2L-CHB	3L-NPC	4L-NPC	3L-FC	Dual-Supply
Number of switches	10	20 k [1]	20	30	20	20
Number of Diodes (including antiparallel diodes)	10	20 k	30	50	20 + 5 capacitors	20
Number of needed DC sources and capacitor banks	Single DC source	Isolated DC source to each H-bridge	Single source + two capacitor banks	Single source + three capacitor banks	Single source + two capacitor banks	Two isolated DC sources
Access to dc-link midpoint requirement	No	No	Required	Required	Required	No
Voltage balancing requirement	No	No	Required	Required	Required	No
Voltage stress on each switch [2]	V_{dc}	$\frac{1}{2k} V_{dc}$	$\frac{1}{2} V_{dc}$	$\frac{1}{3} V_{dc}$	$\frac{1}{2} V_{dc}$	$\frac{1}{2} V_{dc}$
Complexity	Simple	Moderate	Moderate	Moderate	Complex	Complex
Power density	Baseline	Medium-Low	Medium-Low	Low	Medium-Low	Medium-Low
Advantages	+ Simple + Easy control	+ High voltage-levels + Low switching frequency + Low voltage power switches + Low THD	+ 3-level voltage + Well-proven technology + Lower dv/dt	+ 4-level voltage + Well-proven technology + Lower dv/dt compared to 3L-NPC	+ 3-level voltage + No clamping diodes + Additional switching states maintaining capacitors balance	+ Low voltage applications + No balancing voltage needed
Disadvantages	- Only for lower voltage applications - High THD - High dv/dt and EMI - High power switches stress	- Higher number of capacitance/dc-source - Large PCB footprint - Not for regenerative applications	- Clamping diodes - Uneven heat distribution - Voltage unbalance	- Clamping diodes - Uneven heat distribution - Voltage unbalance - High number of components	- Capacitors are more expensive - Complex start-up - More difficult control	- Increased number of components
Technology status for EV applications	Already manufactured	Only research area				

[1] k is the number of cells. [2] Assuming using the same battery voltage V_{dc} with a battery pack arrangement

4.6. More Topologies

There are additional multilevel inverter topologies that have been discussed in the literature [72–75], but they may not be as well-known as the ones mentioned in previous sections. As an example, the seventeen-level inverters with reduced components have a hybrid cascaded H-bridge topology [74], a packed U cell (PUC) multilevel inverter [73], and a three-level dual output voltage (TL-DOV) inverter. Certain topologies have received particular attention and will be described briefly here below:

- The Five-Level H-Bridge NPC (5L-HNPC): 5L-HNPC consists of two 3L-NPC legs arranged in an H-bridge configuration per phase, as depicted in Figure 15a [76–78]. It is an adapted version of the CHB with only one cell per phase, but it utilises NPC legs instead of 2L-VSC legs. The combination of the three levels of each leg of the NPC results in five different output levels. Similar to CHB, it requires isolated dc sources for each H-bridge to avoid short circuits of the dc-links. However, similar to the CHB, this topology results in a significant improvement in the grid-side currents.
- The three-level neutral point piloted (3L-NPP): The topology consists of a 2L-VSC in which the output phase nodes are connected to a midpoint in the dc-link via a bidirectional switch [70,79]. This allows for the creation of an additional voltage level, similar to the 3L-NPC. However, the disadvantages include the need for snubber protection on the series-connected devices and the use of a bidirectional switch that requires a special switching sequence. The 3L-NPP is shown in Figure 15b, c with one switch per leg and two switches per leg, respectively.
- The modular multilevel converter (MMC): is also known as M2C. Basically, the MMC is composed of single-phase, two-level voltage source converter (2L-VSC) legs, which are also known as half-bridges, connected in series, as illustrated in Figure 15d [80–82]. As the capacitors are floating, a voltage balance control must be implemented to maintain a constant voltage level for each one [81].

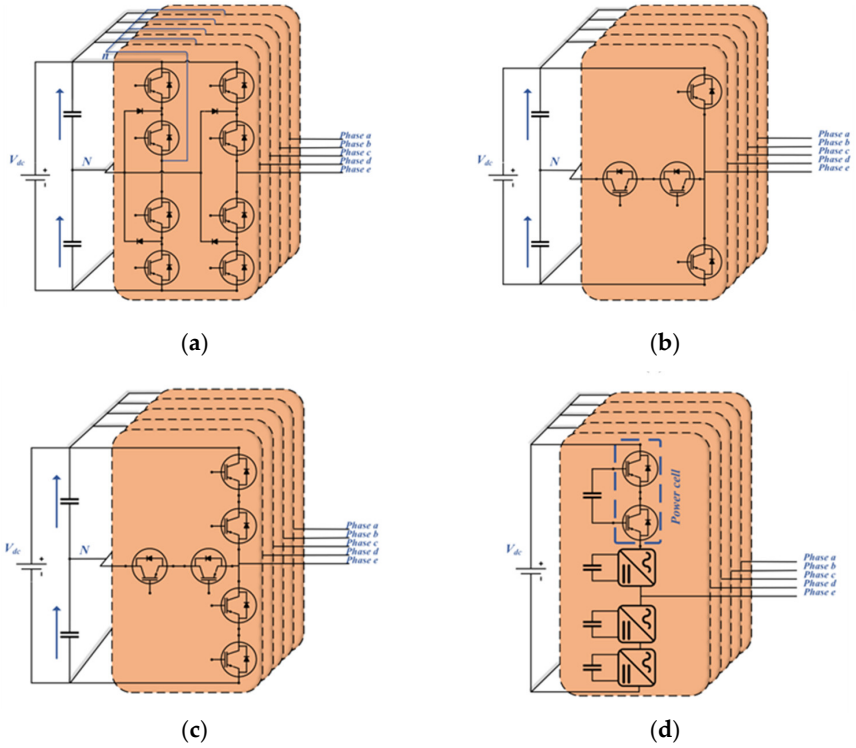

Figure 15. More topologies for five-phase drives: (**a**) 5L-HNPC; (**b**) 3L-NPP; (**c**) 4L-NPP; (**d**) MMC.

5. Drive Topologies for Six-Phase Machines

This section will cover various topologies used for six-phase MPDs that can be exploited in EV applications. These topologies are all DC-AC converters, as the energy storage system in traction applications is typically battery packs.

5.1. Two-Level Six-Phase VSC

The two-level, six-phase topology is the most investigated topology in all the literature due to its simple structure. The structure of a two-level, six-phase inverter is shown in Figure 16.

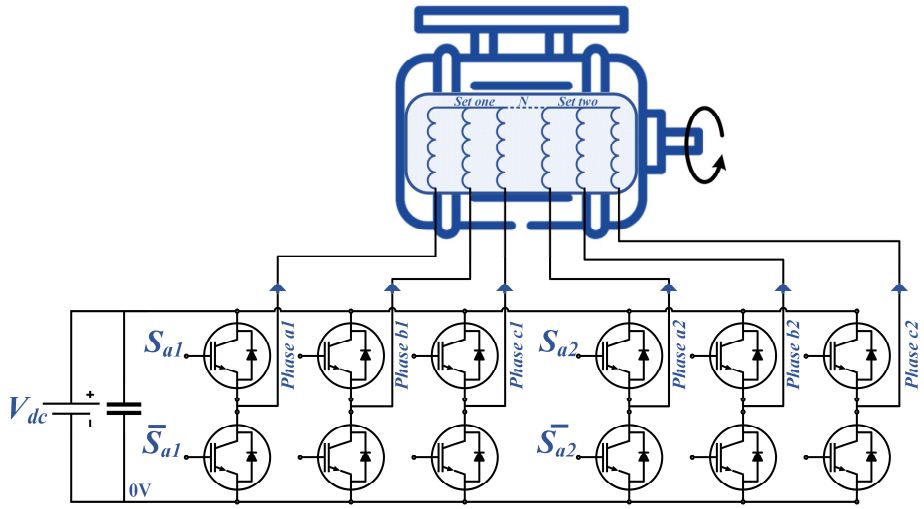

Figure 16. Two-level converter topology for a six-phase voltage source drive.

5.2. Reduced Switch-Count Inverters for MPDs

One of the developmental trends followed by researchers while designing power converters is to reduce the number of passive and active components used in order to lower the overall costs, improve the power density, and reduce the size of converters. These topologies are called reduced switch-count topologies.

5.2.1. Nine-Switch Inverter (NSI)

In the six-phase machines, one of the topologies that have been widely studied in the literature is the nine-switch inverter (NSI) [83–86].

Unlike the conventional topology of the two-level, six-phase motor drive system, in which the leg is constituted by one upper and one lower switch and where 12 power switches (six legs) are employed, the nine-switch inverter topology is composed of upper switches, medium switches, and lower switches. As shown in Figure 17, the converter consists of upper switches S_1, S_2, and S_3, medium switches S_a, S_b, and S_c, and lower switches S_4, S_5, and S_6, where each pair of phases shares the same converter. The nine-switch inverter structure consists of two three-phase inverters combined with three common switches (S_a, S_b, and S_c). The upper portion in Figure 17 is equivalent to the first inverter, and the lower part is equivalent to the second inverter. The first equivalent inverter consists of switches S_1, S_2, and S_3, and S_a, S_b, and S_c. The equivalent second inverter consists of switches S_a, S_b, and S_c and S_4, S_5, and S_6.

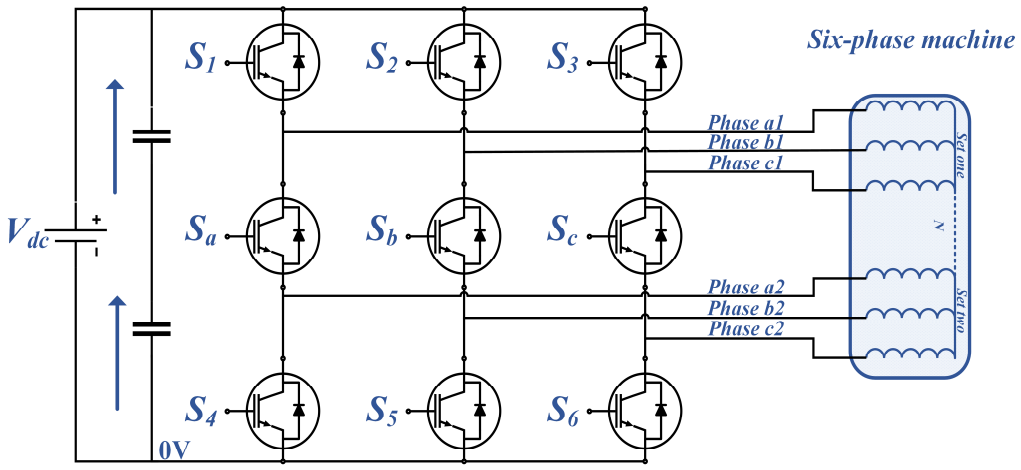

Figure 17. Six-phase, nine switch topology for a six-phase voltage source drive.

The concept of NSI is to exploit its middle switches to replace the lower switches of one of the three-phase inverters and the upper switches of the second three-phase inverter. The middle switches have a switching frequency that is twice that of the other switches, which results in total losses equivalent to those of the conventional 12-switch topology.

There are only three valid states for each phase leg of the nine-switch converts. The switching details for the first leg are described as follows [84]:

- State 1: Both phases from the same phase leg tie to the upper dc-rail by turning $S_1 = S_a$ = ON;
- State 2: Phase a_1 ties to the upper rail, while phase a_2 ties to the lower rail by turning $S_1 = S_4$ = ON;
- State 3: Both phases tie to the lower dc rail by turning $S_a = S_4$ = ON.

In total, only three out of eight (2^3) possible gating combinations are used by the three aforementioned states, where two ON signals are distributed among the three switches of S_1, S_a, and S_4 per phase leg. The other three combinations with only one ON signal can happen during dead time, inserted to protect the converter against the short-circuit combination of accidentally turning ON all three switches. However, an all-OFF combination

should generally be avoided as well, since it leads to uncontrollable phase outputs, whose values are passively determined by the directions of current flow [84].

In order to control the nine IGBTs, the PWM is the easiest way to generate the gate control signal.

The middle switches (S_a, S_b, and S_c) are controlled by simply applying the logical *XOR* operator to the signals derived for the upper switches (S_1, S_2, and S_3) and lower switches (S_4, S_5, and S_6). The gating signals of the upper and lower switches are obtained as for conventional configuration PWM. The insertion of dead time to protect the converter against any accidental short-circuits is automatically guaranteed with the *XOR* control command applied to the middle switches [83].

In order to guarantee that two sets of the three-phase signals required by a six-phase machine are correctly generated by the nine-switch converter, it is necessary to ensure that the upper reference voltage v_{a1}^* is always placed above the lower reference voltage v_{a2}^* without crossover intersection. In this case, the amplitude of both sets of three-phase voltages must have the same amplitude, while presenting different phase displacements α (30° and 60° for asymmetrical and symmetrical machines, respectively).

A direct consequence of this no crossover intersection between the upper and lower reference voltages (v_{a1}^* and v_{a2}^*) is that the maximum modulation index will be limited by the amplitude sum of both references, and the modulation index will be lower compared to the conventional six-leg voltage source inverter, as observed in Figure 18.

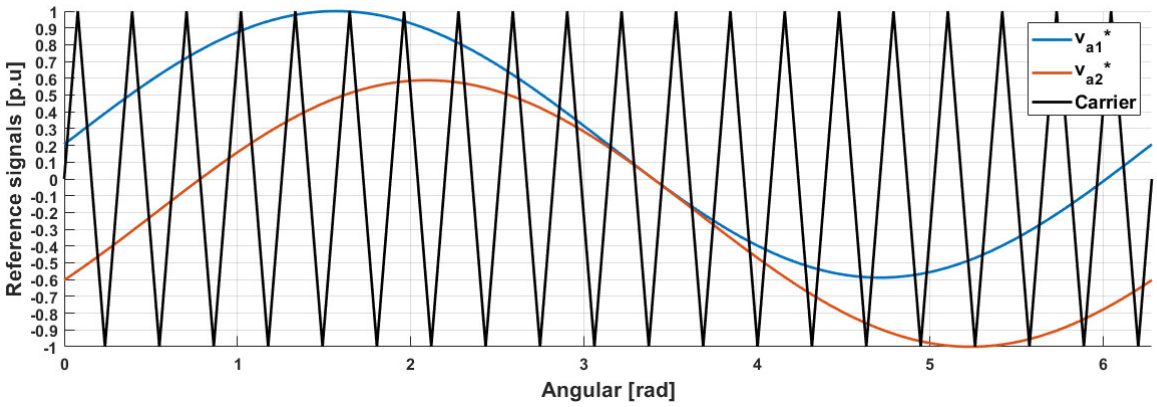

Figure 18. Carrier wave and reference voltages v_{a1}^* and v_{a2}^* for nine-switch converters.

As defined in [84], $M \leq \left(1 + \sin\left(\frac{\alpha}{2}\right)\right)^{-1}$, where M is the modulation index and α is the displacement between the two sets of the three-phase outputs. In considering α = 30° and α = 60°, the maximum modulation indeces are $M = 0.794$ and $M = 0.667$ for asymmetrical and symmetrical machines, respectively. In an asymmetrical machine, the modulation index is higher than the observed one for the symmetrical machine, since the phase displacement is lower.

Figure 19 shows the block diagram of the PWM strategy employed for the nine-switch converter. In this figure, V_{offset} is the voltage used to guarantee no intersection, and it depends on the six-phase machine employed. In the asymmetrical machine, $V_{offset} = 0.2\ pu$, while for the symmetrical one, $V_{offset} = 0.33\ pu$, with the amplitude of the triangular waveform equal to 1 pu. In the event that the same modulation index is used for both motor drive systems, the dc-link voltage of the nine-switch converter must be increased to guarantee the same voltage is applied to the machine. Such an increase will be 20% and 33% for the asymmetrical and symmetrical machines, respectively.

In [84], the optimal pulse-width modulation of the nine-switch converter is studied. The NSI can either operate at a single common frequency (CF) or at different frequencies (DFs). In [85], an analysis and comparison of the Zero Space Vector PWM (ZSVPWM) with respect to the conventional SPWM technique for the nine-switch inverter topology are presented.

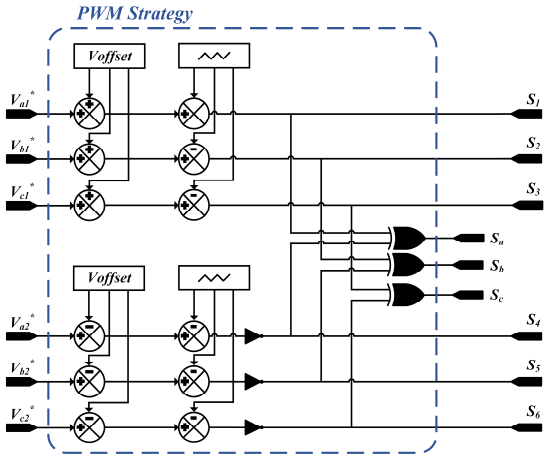

Figure 19. PWM control strategy for nine-switch converters.

In [87,88], predictive current control (PCC) and predictive torque control (PTC) are presented, respectively. The predictive control is characterised by fast dynamics, the absence of voltage modulators, and the easy incorporation of nonlinearities and system restraints, which makes it an interesting control strategy. In [89,90], the direct torque control (DTC) is presented.

5.2.2. Five-Leg Inverter (FLI)

The five-leg inverter (FLI) is another topology with a smaller number of switches [91–94]. In this paper, two topologies of five-leg inverters are presented. These topologies can be obtained either by using the capacitor midpoint connection or by sharing one of the converter legs. The first topology with a shared converter leg was initially developed to control two separate three-phase drives. However, the five-leg inverter-fed dual three-phase machine can be regarded as the specific case of a five-leg inverter-supplied dual six-phase machine [94,95].

The first topology is presented in Figure 20, where two phases share the common leg. The common-leg maximum current is doubled compared with the current flowing in all switches of the 2-VSI or in other leg switches for the FLI [93]. A comparison of the characteristics of a five-leg inverter, a nine-switch inverter, and a 2-VSI is presented in [93]. The analysis shows that even though the two-level VSI has more switches (12 compared to 10), the total 2-VSI inverter losses and the switch capacity are lower compared to the FLI and the NSI for fixed inverter parameters. Basically, the losses in the FLI are lower compared to the nine-switch topology, but the NSI has merit because the number of switches can be decreased compared to the 2-VSI and the FLI.

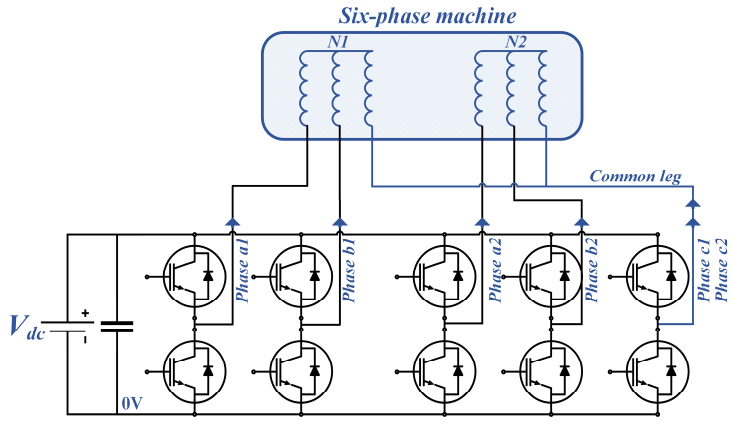

Figure 20. Topology 1: Structure of a five-leg inverter for a six-phase machine.

The second topology, shown in Figure 21, involves connecting one machine phase to the midpoint of the dc-link. The main challenge with this approach is maintaining balance at the mid-point voltage [92].

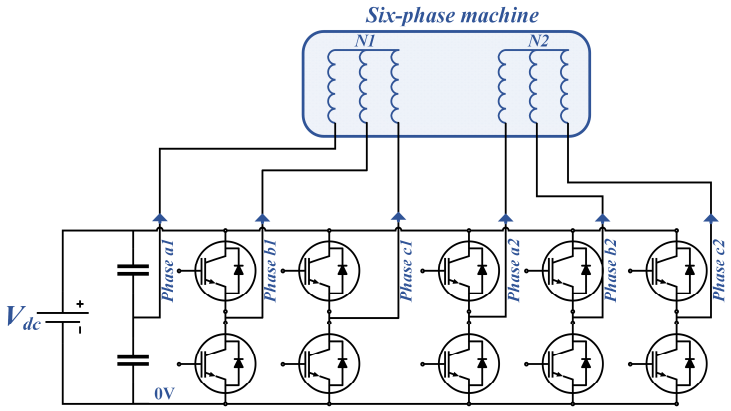

Figure 21. Topology 2: structure of a five-leg inverter for a six-phase machine.

5.2.3. Four-Leg Inverter

Another topology has been studied in [96–98], aiming for low-cost, low-volume, and loss reduction. This topology is a four-leg inverter and is illustrated in Figure 22.

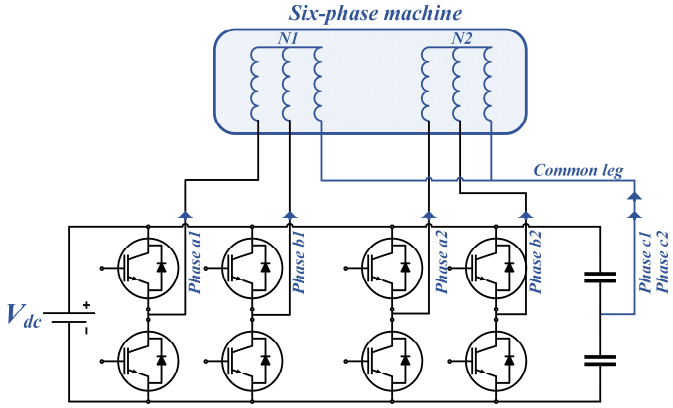

Figure 22. Structure of a four-leg inverter for a six-phase machine.

The four-leg inverter is a single inverter that can drive two motors independently or a dual six-phase motor. The four-legged topology consists of four legs, with one leg using two capacitors connected in series.

5.3. Six-Phase Dual Supply Open-End Winding Drives

The dual-supply inverter topology has been extensively investigated in the last two decades, and this topology is only used in open-end winding configurations. As mentioned for the five-phase drive, this topology does not need a capacitor voltage balancing technique if it is supplied by isolated dc sources and does not utilise a DC bus capacitor.

In the literature, several topologies are introduced based on the type of supplies used and the method of connection; the topologies are as follows:

- Topology I (dual supply topology): the two-sided supplies are used to power two six-phase inverters, with each phase winding connected to a converter output from both phase terminals.
- Topology II: this topology utilises a single DC supply to power the two inverters in a five-phase drive in order to eliminate the common-mode voltage by means of SVPMSM [99].

- Topology III: this topology involves four three-phase inverters and two dc-link supplies that are connected from both sides with a capacitor shared by the middle inverters [100,101].

Topologies I, II, and III are illustrated in Figure 23, Figure 24, and Figure 25, respectively.

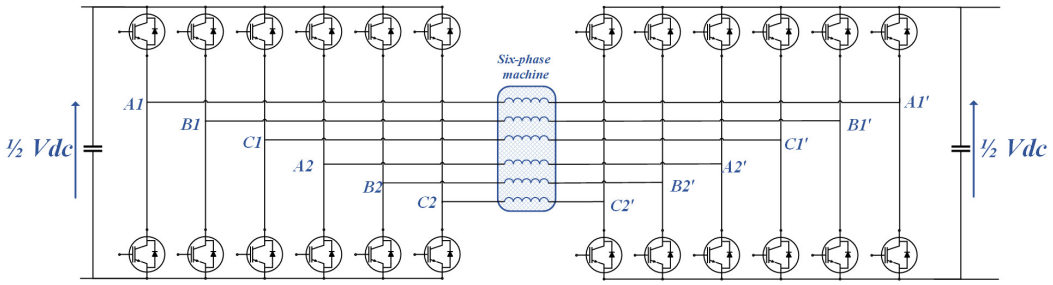

Figure 23. Open-end winding, six-phase topology with dual two-level inverters and dual dc sources (topology I).

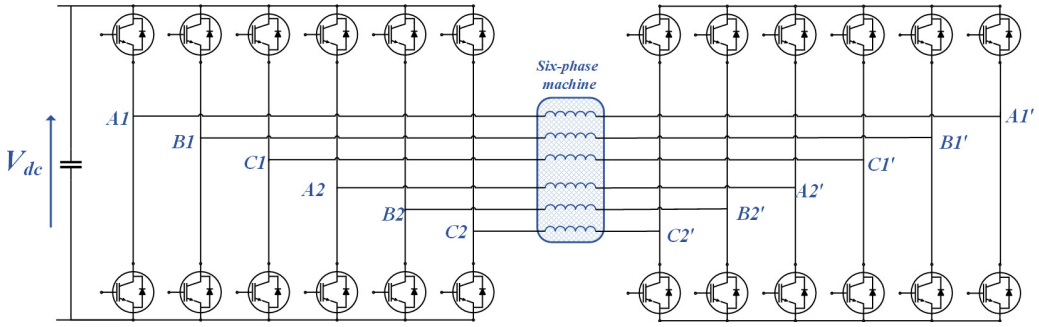

Figure 24. Open-end winding, six-phase topology with dual, two-level inverters and a single dc source (topology II).

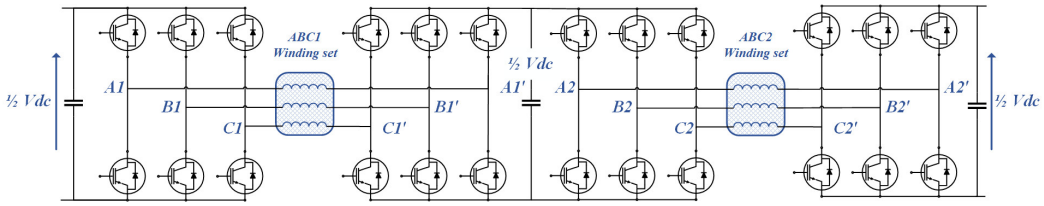

Figure 25. Open-end winding six-phase topology with quadruple two-level three phase inverters and triple dc sources (topology III).

It should be noted that the dual supply inverter, consisting of two two-level six-phase voltage source inverters fed from two equal and mutually isolated dc voltage sources, has the same performance as a three-level VSI in single-sided supply mode [102].

In [103], the peak-to-peak ripple amplitude of the dual-supply inverter (Topology I) with different modulation indices is compared with the corresponding ripple of the single two-leg inverter, considering the same voltage and power motor ratings. The theoretical and numerical results show that the normalised ripple of the dual supply inverter is lower for the whole modulation index range.

As explained before, the major drawback of the six-phase machine is the large harmonic currents ($6n \pm 1$, n = odd order) in the stator windings due to the absence of back-emf for these currents. In order to address this issue, one simple strategy has been to use inductive filters between the inverter and the six-phase machine, but the inductive filters are bulky and costly. As a result, four three-phase inverters (topology III) are introduced in [101] to suppress mainly the fifth and seventh harmonics. Another topology, which will be referred to in this article as topology IV, is similar to topology III, but the

middle capacitor with a voltage balancing strategy [100] is replaced with a dc-link power supply in the middle in order to reduce the cost and size of the drive.

In [104], the authors compare the performance of carrier-based pulse width modulation (PWM) techniques for symmetrical and asymmetrical six-phase open-end winding drives supplied by two-level six-phase voltage source inverters (VSIs).

5.4. Multilevel Inverters

AC motor current ripple in electric vehicles is a source of electromagnetic interference and audio noise, both from the inverter-motor power connection cables and from the motor itself. By increasing the inverter switching frequency, the ripple amplitude is reduced, but the drive efficiency decreases due to the proportionally increased switching losses. A viable solution to reduce the current ripple amplitude is to introduce a multilevel inverter.

The three-level NPC inverter topology is shown in Figure 26.

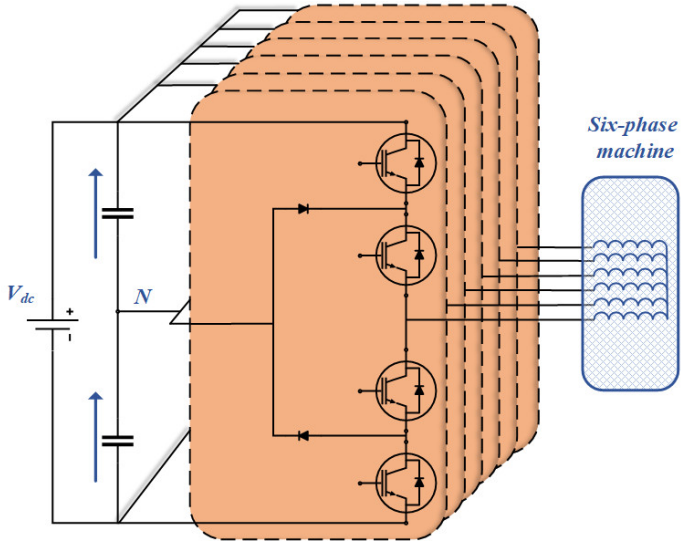

Figure 26. NPC-fed for a six-phase machine.

The modelling and control of the six-phase NPC are investigated in [105–107].

An overview comparison between MPDs for the six-phase machines is summarised in Table 3.

Table 3. Comparison between different converter topologies for six-phase drives.

	Conventional 2-Level	2L 5-Leg	2L 4-Leg	NSC	3L-NPC	Dual-Supply
Number of switches	12	10	8	9	24	24
Number of needed DC sources and capacitor banks	Single source	Topology 1: Single source Topology 2: Single source + two capacitor banks	Single source + two capacitor banks	Single source	Single source + two capacitor banks	Topology 1: two sources Topology 2: single source Topology 3: two sources + extra capacitor bank Topology 4: three sources
Access to dc-link midpoint requirement	No	Topology 1: No Topology 2: Required	Required	No	Required	No
Voltage balancing requirement	No	Topology 1: No Topology 2: Required	Required	No	Required	Topology 1: No Topology 2: No Topology 3: Yes Topology 4: No
Voltage stress on each switch [1,2]	V_{dc}	V_{dc}	V_{dc}	V_{dc}	$\frac{1}{2}V_{dc}$	$\frac{1}{2}V_{dc}$
Reliability	Medium	Low	Low	Low	Low-Medium	High
Complexity	Simple	Moderate	Moderate	Moderate	Complex	Complex
Power density	Baseline	High	High	High	Low	Low
Technology status for EV applications	Already manufactured			Only research area		

[1] Assuming using the same battery voltage, V_{dc}, with a battery pack arrangement. [2] For topology 4, three dc-sources are required ($\frac{Vdc}{2}$), to do so, the battery pack modules' number should be 1.5 times higher.

6. More Multiphase Drive Topologies

6.1. Multiple Three-Phase Drives

In Section 5, the six-phase machines and drives are highlighted, as these machines are the most investigated and studied topologies. In this section, additional multiples of three machines, namely nine, twelve, and fifteen phases, will be briefly covered. Multiple three-phase machines are interesting because one of their main advantages is the ability to use standard three-phase inverters in parallel without the need to make a high-phase number inverter.

In [108], a 5 kW nine-phase reluctance drive is described. The third, fifth, and seventh current harmonics are injected into the stator phase currents to enhance the average torque. The experimental results show that rewinding synchronous reluctance motors to a higher number of phases allows the stator MMF to be reshaped and offers an optimised distribution for air-gap flux, a higher winding factor, and a higher value for the fundamental component of the MMF with lower harmonics [108,109].

The nine-phase PMSM drive based on triple three-phase back-to-back voltage source converters for an ultrahigh-speed elevator is introduced in [110]. The ultrahigh-speed elevator moves more than 1000 m/min [110], which means a high-power traction system with a peak power rating of more than 1 MW is needed. This high power can be achieved only by using a large number of phases, such as nine-phase topologies, to reduce the current rating of each phase. Moreover, because nine-phase motors have lower torque ripple characteristics and open-phase fault tolerance, it becomes possible to improve the ride comfort and safety of the passengers, especially for elevator applications. Within the same framework, the operation in fault condition is addressed in [111,112]. In order to control the nine-phase motor, a mathematical model is needed. For this reason, a simplified model using vector space decomposition is investigated in [113].

The twelve-phase drives are covered in [114,115]. In controlling the twelve-phase drive, the easiest and most common way is to use four two-level, three-phase VSI [114]. In [115], a separate double-winding 12-phase BLDC drive fed from an individual H-bridge inverter is studied. For example, by using a separate inverter for each phase, it is possible to repair or replace the converter for one phase in case of any fault in the inverter module. Moreover, the conspicuous reduction of torque ripple for an increased number of phases has also been verified.

In addition, the fifteen-phase drives have been studied in different papers [116,117]. A high-power 20 MW driver for advanced fifteen-phase ship propulsion induction motors was developed in [116]. A 20 MW PWM driver is designed with a special third-order harmonic injection. The AC voltage from a 10 kV electric network is supplied to three groups of five-phase H-bridge inverter units after being stepped down and rectified by three *3/6* phase transformers with primary windings that mutually differ by 10° in terms of phase shift. While considering the output waveform quality, the neutral-point-clamped (NPC) five-level H-bridge main circuit topology is applied to every inverter unit, and a single NPC five-level H bridge inverter unit for the 20 MW PWM driver is mainly composed of 4 diode modules and 8 IGBT modules and drivers. The modelling and control of a fifteen-phase induction machine for marine applications under a one-phase open circuit fault are addressed in [117].

6.2. Seven-Phase Drives

The seven-phase voltage source inverter topologies are covered in [118–123] and shown in Figure 27. In the majority of research papers, the two-level voltage source inverter is used.

The space vector modulation of a seven-phase voltage source inverter with an investigation on the maximum value of the modulation index for sinusoidally balanced output voltage is presented in [118]. In particular, the proposed SVM strategy univocally selects the inverter switch configurations among the $2^7 = 128$ possibilities by privileging the space vector on the first *d-q* plane. The resulting switching patterns, collected in a general switching table, include six active and two null configurations, with a single leg commutation for

each configuration change. In [119], discontinuous space vector strategies for a seven-phase voltage source inverter are investigated. The proposed strategy offers the best utilisation of available dc-link voltage and offers nearly sinusoidal output. A significant reduction in switching losses is observed.

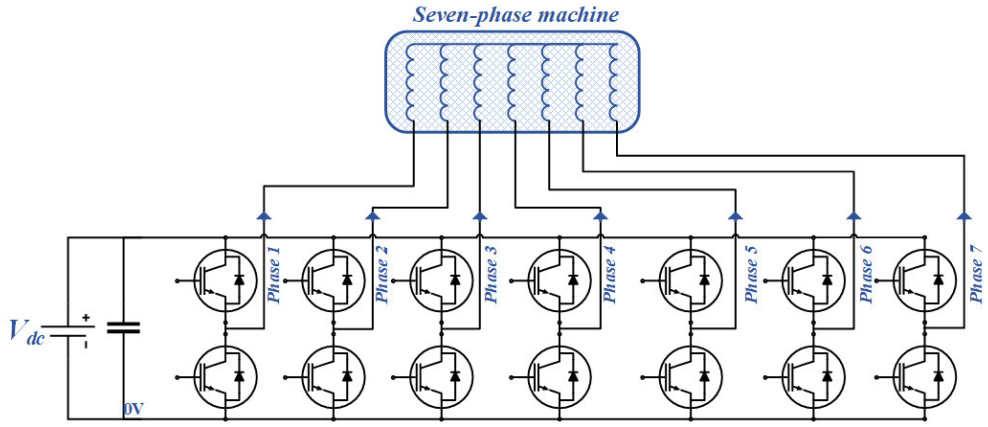

Figure 27. Two-level converter topology for a seven-phase voltage source drive.

A general modulation strategy for seven-phase inverters that combines the multiple space vector representation with traditional carrier-based pulse width modulation is studied in [123], and the investigation shows that the proposed modulation technique is able to fully exploit the input dc-voltage and can enhance the torque density.

Moreover, the multilevel topologies are also investigated to be used for seven-phase drives, and precisely the three-level seven-phase voltage source converter with SVPWM is covered in [123,124]. The use of a three-level inverter is very complicated, especially in generating the space vector strategies, which stem from the nature of the multiphase systems. Increasing the number of levels from two to three increases the number of switching states from $2^7 = 128$ to $3^7 = 2187$ and the number of orthogonal planes from two to three.

A matrix AC-AC converter using carrier based PWM is presented in [121], and the space vector PWM technique is in [122]. The studied matrix converter is illustrated in Figure 28.

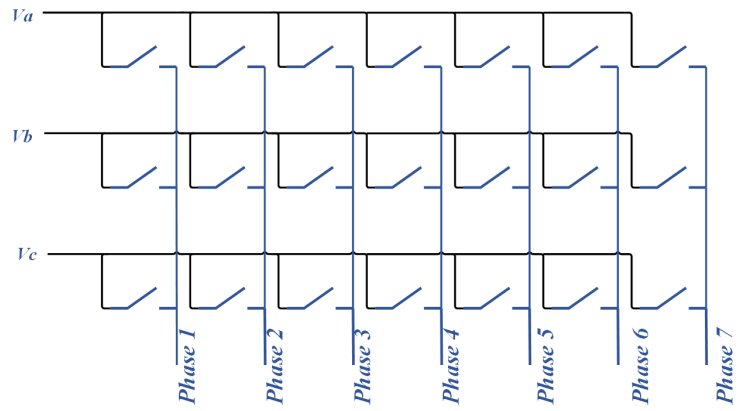

Figure 28. The topology of 3×7 matrix converter.

6.3. Eleven-Phase Drives

The eleven-phase converter for the induction machine is studied in [125,126], where the two-level topology is used. The steady-state analysis and performance evaluation of an eleven-phase induction machine using a selective harmonics elimination (SHE) technique are compared with a quasi-square inverter output. In the case of high mechanical loads with high amperes per torque ratio, the experimental results show that the torque density

is better with a square-wave supply than injection SPWM with lower order harmonics, as in multiphase machines, where the harmonic currents contribute positively to the torque production. Moreover, as SPWM has a limitation in medium-voltage drives due to its high switching frequency, using square-wave instead of SPWM with SHE will reduce the phase current, torque pulsation, and induced rotor harmonic currents and significantly reduce switching loss because of the reduced switching frequency.

7. Control Methods and Modulation Techniques for Multiphase Machines

In this section, the most common control methods of MPDs and their modulation techniques are discussed.

7.1. Control Strategies for MPDs

The different control methods as field oriented control (FOC), direct torque control (DTC), and more recent methods such as MPC are covered in this section below.

7.1.1. Field Oriented Control (FOC)

Field-oriented control (FOC) is a widely utilised vector control method for three-phase machines and multiphase machines as well. The main difference is that for the multiphase machine, more subspaces are needed to model the machine, leading to the need for additional PI current controllers to eliminate these currents. FOC is known for its good transient performance. The key to implementing FOC is to either measure the rotor angle using position sensors, such as an optical encoder or resolver (in the case of sensored control) or estimate it in the case of sensorless control. The rotor angle is utilized to decompose the current components into the torque and flux controlling components. The estimation of the rotor flux angle for an induction machine is more complicated as the slip between the rotor and stator flux speeds should be taken into consideration. Position estimation for sensorless FOC of five-phase PMSMs is covered in [127], with a focus on estimating rotor position and speed from motor back-EMF using a sliding mode-based observer and adaptive band-pass filter.

In [30,128–134], the attention has been mostly focused on the design of the control strategy to guarantee a smooth postfault operation of the five-phase drive, where FOC has been used with a cascaded inner current control loop and an outer speed/torque control loop. The different objectives can be achieved by using FOC control, such as sinusoidal magnetomotive force [30,128], minimum torque ripple [129,130], minimum torque derating [131], or minimum copper losses [132,133].

7.1.2. Direct Torque Control (DTC)

In DTC, the stator flux and torque can be controlled directly by properly selecting the voltage vectors from a predefined switching table. The main advantages of DTC are its very fast torque response and the low complexity of the control algorithm because no coordinate transformations are needed all calculations are done in a stationary coordinate system. Major drawbacks of a DTC scheme are high torque and flux ripples [135].

7.1.3. Model Predictive Control (MPC)

Nowadays, with the development of faster and more powerful microprocessors, model predictive controls (MPC) represent one of the most competitive solutions as an alternative to conventional feedback control schemes, especially when faster dynamic response is needed [136]. This control method was first introduced in [137]. The MPC has several advantages that make it appropriate for MPD control, including the possibility of being applied to a variety of systems and the ease with which constraints and nonlinearities can be included. The multivariable case can be considered, and the resulting controller is easy to implement [138]. The concept of MPC is easy to understand; the system model will be used to predict the future behaviour of the controlled variables. This predicted information is used by the controller to obtain the optimal actuation, according to an optimization

criterion. In using predictive control, it is possible to avoid the cascaded structure that is typically used in a linear control scheme, obtaining very fast transient responses. The use of MPC for six-phase machines is discussed in [139–141]; for five-phase machines, see [142,143]. One major challenge with MPC is the requirement of the exact model, drive parameters, and increased sampling periods as a large number of calculations are necessary.

Table 4 shows a comparison between different control methods. For many years, the FOC and DTC methods have been widely utilised in both academic and industrial applications. However, the MPC method is a promising and relatively new method compared to FOC and DTC, as it is simple to implement, the modulation scheme is already included in the control method, it does not require tuning of controller parameters, and it has a faster transient response.

Table 4. Comparison between different control methods.

	Scalar	**FOC**	**DTC**	**MPC**
Use of PI controllers	Speed controllers: no	Speed controllers: yes	Speed controllers: yes	Speed controllers: yes
	Current controllers: no	Current controllers: yes	Current controllers: yes	Current controllers: no
Transient response	Very slow	Slow	Fast	Very fast
Dynamic performance	Low	Medium	Medium	High
Modulation technique	No modulation needed	CBPWM SVPWM	CBPWM SVPWM	Signals directly from controller
Implementation and complexity	Simple	Complex	Moderate	Moderate
Sensitivity to system parameters	Medium	Sensitive	Sensitive	Very sensitive

Some reference papers that covered the MPDs control for five-phase and six-phase are summarized in Table 5.

Table 5. Different possible control methods for five and six-phase machines.

Machines	**Type of Machines**	**Example of Possible Control Strategy**
Induction machines	Five-phase machines	Model-based predictive current control [144]
	Six-phase machines	Open loop *v/f* scalar control [52,53] Field oriented control (FOC) [145,146] Direct torque control (DTC) [147]
PMSMs	Five-phase machines	Open loop *v/f* scalar control [148] Field oriented control (FOC) [127,146] Direct torque control (DTC) [135]
	Six-phase machines	Field oriented control (FOC) [149] Direct torque control (DTC) [150]

Another control strategy that can be used for multiphase machines is sliding mode control (SMC). Sliding mode presents robustness and takes into account the switching nature of the power converters [138]. In comparison to model-predictive control, MPC is a model-based control, but SMC is a model-free control. In other words, SMC is mainly used for uncertain plants. The SMC is covered for five-phase machines in [151,152] and six-phase machines in [153]. Other control schemes found in the literature include neural networks, neuro–fuzzy system, and other advanced control techniques.

7.2. Modulation Techniques for MPDs

The power quality of an inverter is highly influenced by the electromagnetic noise generated by the current harmonics from inverter operation. The amplitude and the frequency of these harmonics depend on the modulation technique [154]. The same basic modulation techniques used in three-phase systems can also be applied to multiphase inverters. This section presents the most common modulation techniques used in multiphase drives.

7.2.1. Carrier-Based PWM (CBPWM)

The carrier PWM is the most widely used and simplest carrier-based modulation of three-phase inverters, which can also be utilised to operate multiphase drives. The implementation of the CBPWM technique involves the use of reference signals, which are generated from the control scheme. These reference signals are then compared to a carrier signal, and the resulting output signals are used to activate the switches of the converter. CBPWM is an easy-to-use modulation technique for controlling the multiphase converter. This simplicity, in addition to its reliability, makes this technique suitable for EV applications. However, despite its simplicity and reliability, the CBPWM is limited in terms of control flexibility to enhance the converter's performance, such as reducing the total harmonic distortion. This modulation technique has been discussed in various literature, including [52,53].

7.2.2. Space-Vector PWM (SVPWM)

The SVPWM technique, which is widely utilised in three-phase machines, has garnered significant attention due to its high switching efficiency and low losses, leading to improved power conversion efficiency, reduced harmonics, and ease of implementation.

The SVPWM technique in multiphase drives is complex due to the numerous switching states and voltage space vectors that must be simultaneously considered in multiple planes. Therefore, CBPWM methods are more practical due to their simplicity [63]. In [63], a comparison of CBPWM and SVPWM methods shows that CBPWM is capable of achieving the same level of performance as the SVPWM method while requiring a highly reduced computational burden. In [155], a decoupled SVPWM algorithm that views the inverters as individual two-level converters for open winding five-phase machine topology is discussed. The method is based on sharing the reference voltage between two inverters in the same ratio as the dc-link voltages, with both inverters having the same switching frequency. SVPWM for split-phase induction motor drive is covered in [156].

Furthermore, despite its complexity, SVPWM remains attractive for use in multiphase traction inverters due to its improved utilisation of the DC bus voltage, lower harmonic components, improved fault tolerance through the use of redundant switching states for the same voltage vector, and reduction of the circulation currents and, as a consequence, the ohmic losses.

7.2.3. Zero-Sequence Injection (ZSI)

This modulation technique is adapted for an asymmetrical six-phase machine. The idea consists in the utilisation of two three-phase modulators whose reference inputs are shifted by 30 degrees [154] and by adding a certain zero-sequence signal that divides the null vector time equally between the two zeros to reduce the current ripple, improve dc-supply utilization, and extend the linear region of the inverter. [157]. The double zero-sequence injection for six-phase machines is covered in multiple papers, such as [52,145,154,158,159].

7.2.4. Level-Shifted PWM (LS-PWM) and Phase-Shifted PWM (PS-PWM)

The LS-PWM and PS-PWM are extensions of carrier-based sinusoidal PWM used for the NPC and for multicell converters (CHB and FC, respectively). The PS-PWM assigns a pair of carriers to each cell of the CHB and FC, and a phase shift among the carriers of the different cells introduces asynchronism, which generates the stepped waveform. In this case, the advantage lies in the power being evenly distributed among the cells across the full range of the modulation index, which enables correct operation of the multi-pulse rectifier configuration of the CHB and a natural balancing of the capacitors in the FC.

7.2.5. Recent Advances in Modulation Methods

Several researchers focused on the analysis and comparative study of PWM modulation techniques for six-phase machines, as presented in [160]. The comparison between the modulation strategies is based on several criteria: current harmonic minimization,

hardware and software implementation complexity, and low-cost fixed-point DSP platforms [160]. The general conclusion that can be extracted from the literature is that the space vector modulation is simple to implement but low order harmonic currents will be present because the modulation only controls the (α, β) subspace, which leads to extra losses in the machine and thus reduces the multiphase drive efficiency. By using the vector-space decomposition technique, the harmonics could be minimized. The double zero-sequence injection techniques offer similar good results from the point of view of harmonic minimization, and the implementation complexity is significantly reduced compared to the space vector decomposition technique. Consequently, these digital modulation techniques can be easily implemented with low-cost fixed-point DSP controllers.

8. Current Status, Research Challenges, and Trends of MPDs

8.1. Current Status in the Use of EVs with Integrated MPDs

One industrial manufacturing company that uses MPDs is DANA TM4, which produces SUMO^{TM} MD, a PMSM six-phase drive for heavy-duty EVs. Figure 29 shows the TM SUMO^{TM} MD MPD.

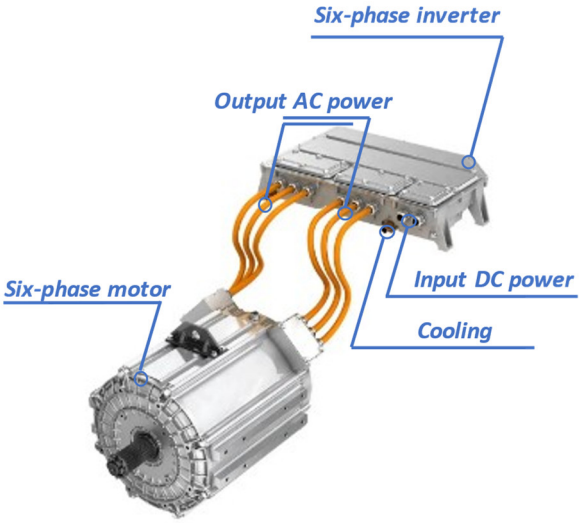

Figure 29. DANA TM4 SUMO^{TM} MD six-phase drive [161].

The TM4 SUMO^{TM} MD comes in several models with a continuous power between 100 kW and 155 kW (peak power range between 162 kW and 265 kW), a continuous torque ranging from 680 Nm to 970 Nm (peak torque from 1590 Nm to 2760 Nm), and a maximum speed of 3700 rpm. The product series is designed for use in medium- to heavy-duty vehicles.

The second series is called SUMOTM4 HP. The TM4 SUMOTM MD has different models with a continuous power range between 170 kW and 430 kW (peak power range between 220 kW and 540 kW), a continuous torque ranging from 624 Nm to 2050 Nm (maximum torque ranging from 915 Nm to 2500 Nm), and a maximum operating speed of 4000 rpm. The SUMOTM4 HP series has a higher power rating, which makes it suitable for heavy-duty and off-highway applications.

The DANA TM4 also provides nine phase machines called SUMO^{TM} HD that are used for heavy-duty applications. The drive SUMO^{TM} HD is shown in Figure 30. SUMO^{TM} HD drives offer high characteristics, including a peak power output of up to 370 kW, a peak torque of up to 3445 Nm, and a maximum operating speed of up to 3400 rpm.

Tron-e uses a 230 kW multiphase synchronous PM machine in its nine- and eleven-meter electric buses, as depicted in Figure 31.

Recently, multiphase machines have also been proposed as a potential solution for oil and gas pump applications [163], electric ships [164], and voltage regulation [165].

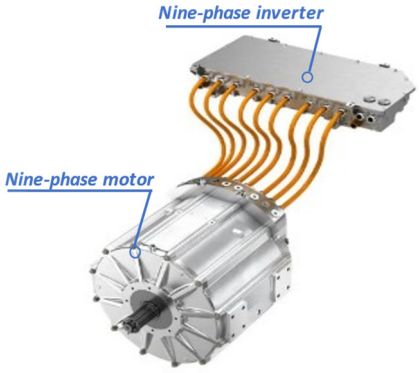

Figure 30. DANA TM4 SUMO^{TM} HD nine-phase drive [161].

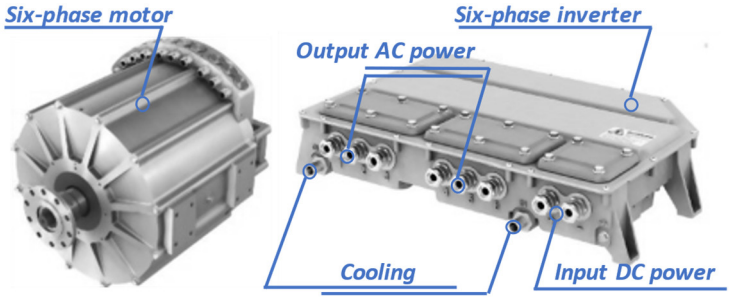

Figure 31. Multiphase drive for an electric bus by Tron-e [162].

8.2. Wide Bandgap (WBG) for MPDs

The evolution of the power converter topologies, including their power capabilities, efficiency, reliability, cost, and performance, is directly related to the progress made in power semiconductor devices [166], which are the core of the drives.

The most commonly used semiconductor device is the power diode, which is widely used for passive rectification and as a freewheeling device. The thyristor, also known as the silicon-controlled rectifier (SCR), is an early high-power device with control capabilities. Presently, insulated gate bipolar transistors (IGBTs) and metal-oxide-semiconductor field-effect transistors (MOSFETs) are the dominant technologies used for power electronics. IGBTs are generally more suitable for high-voltage, high-current applications, while MOSFETs are more suitable for high-frequency switching applications. Table 6 presents a comparison of the different power devices, including their ratings and key features.

Table 6. Comparison of semiconductor power switching suitable for MPDs.

	Diode	Thyristor	SI IGBT	SI MOSFET
Max. voltage	8.5 kV at 1.2 kA	12 kV at 1.5 kA	6.5 kV at 0.75 kA	1 kV at 0.2 kA
Max. current	9.6 kA at 1.8 kV	5 kA at 0.4 kV	2.4 kA at 1.7 kV	1 kA at 0.2 kV
Features	(+) Very high-power (+) Reliable (proven) (−) Conduction losses (−) Reverse recovery current	(+) Very high-power (+) Low losses (+) High overload (−) Slow	(+) Reliable (proven) (+) Fast (+) Self-commutated (−) Medium power	(+) Reliable (proven) (+) Very fast (+) Self-commutated (−) Medium power

The power electronics industry is moving towards the use of wide bandgap devices, which are the next generation of technology in this field due to their superior material characteristics. Typically, the term "WBG" refers to SiC MOSFETs and GaN HEMTs, which are the most commonly used semiconductor switches in the WBG device market. The wide bandgap (WBG) modules have superior performance compared to traditional silicon modules in terms of losses, breakdown voltage, switching frequency, and the ability to

withstand higher junction temperatures [167]. However, using a WBG device with a high switching frequency at relatively high voltages raises the problem of a high derivative of voltage over time, *dv/dt* [168].

In terms of technology, the GaN semiconductors are considered superior to SiC due to their higher breakdown field, faster switching frequency, and lower resistance when conducting $R_{DS(ON).}$ However, device packaging, gate driver design, and electromagnetic compatibility (EMC) are considered more challenging for GaN HEMTs due to the gate and parasitic ringing that can occur during ultra-fast switching. Additionally, one of the main limitations of GaN HEMTs is their low voltage rating (typically $\leq$ 650 V), which limits their use in traction inverters. Instead, they are mainly used in on-board chargers and DC-DC converters.

The application of WBG devices in the EV industry is covered in [169–171]. The study in [171] covered the design considerations and performance evaluation of 1200 V and 100 A SiC MOSFETs. The experimental results show that the losses of a SiC MOSFET are lower compared to a Si MOSFET for the complete switching frequency domain.

8.3. Reliability of MPDs

The reliability of power electronics in terms of failure largely depends on the quality of the components and the design of the system. Power electronics systems that use high-quality components and are well-designed tend to have higher reliability and lower failure rates. However, power electronics systems are subject to various types of failures, including component failures, thermal failures, and electrical failures. The factors that can impact the reliability of power electronics include the operating environment, the level of stress placed on the system, and the maintenance and upkeep of the system.

Reliability is a very important factor in MPDs, as downtimes represent huge economic losses. In certain situations, the failure of power electronics equipment can result in hazardous conditions for both the equipment itself and any individuals nearby. In order to incorporate fault-tolerant capability into the drive, power converters have used the concept of redundant hardware to step in during failure operations, where an additional power switch was connected in parallel to each device to provide an extra path in case of a failure. This concept is known as "$N + 1$" redundancy. The "$N + 1$" concept has also been used in CHB converters by adding a redundant power cell that can replace a faulty one.

The multilevel converters could be seen as less reliable because of the higher component count, but at the same time, they have more internal redundancies and modular structures that favour fault-tolerant operation. It could be interpreted as having redundant hardware built in that is in use under normal conditions but can serve for fault-tolerant operation.

8.4. Manufacturing Cost of MPDs

The cost of multiphase drives compared to three phase drives should be taken into account when choosing which type of drive is most appropriate for a particular application. While multiphase drives may offer improved performance and efficiency, they may also come at a higher cost. In these situations, the benefits of a multiphase drive may justify the added expense, but in other cases, a three-phase drive may be a more economical choice. The transition from three-phase drives to multiphase drives is likely to occur when the cost difference between the two becomes minimal and the advantages offered by multiphase drives support or facilitate this transition.

According to the U.S. Department of Energy (DOE) and the report published by US DRIVE (Driving Research and Innovation for Vehicle Efficiency and Energy Sustainability) [172], the 2025 technical drive targets are listed in Table 7.

The 2025 power electronics cost and volume targets are influenced by the opportunity to replace silicon switches with WBG devices, which have the potential to reduce the size of power modules while enabling operation at higher temperatures and frequencies. Although WBG devices are more expensive than their silicon equivalents, they can ultimately lead to a decrease in overall power electronics costs due to system cost reductions.

Table 7. U.S Department of Energy (DOE) targets for electric drive systems.

Target		2020	2025	Change
Power Inverter	Cost ($/kW)	8	6	25% cost reduction
	Power Density (kW/L)	4	33	88% volume reduction
Electric Motor	Cost ($/kW)	4.7	3.3	30% cost reduction
	Power Density (kW/L)	5.7	50	89% volume reduction
Power Electronics	Cost ($/kW)	3.3	2.7	18% cost reduction
	Power Density (kW/L)	13.4	100	87% volume reduction

8.5. Challenges and Future Trends

One of the key challenges that hinders the adoption and widespread use of MPDs technology is the availability of traditional three-phase drives. The initial cost of producing new technologies, such as MPDs, is often high compared to the cost of traditional drives that are already readily available. This can make it difficult for manufacturers to justify producing more MPDs, as the cost difference may not be significant enough to be considered a "breakthrough" technology.

Moreover, as shown in previous sections, the MPD topologies require a larger number of power switches compared to traditional three-phase drives. This leads to more costly, complex, and bulky converters, especially for high dc-bus voltage applications that require high-power switches, which are generally more expensive and larger in size.

However, due to improvements in industrial power electronics and the dependence on dc-ac converters in transportation applications, MPDs are predicted to be the next trend in electrification and will be widely used in the future because they enable conversion from dc to any number of phases as long as the inverter is more efficient in terms of overall performance.

In the same context, a potential topology is multiphase, multilevel inverters that can be used with lower power switch devices as the voltage applied to the switch is lower than the dc-bus voltage. Additionally, the high output power quality with low THD makes multiphase multilevel inverters very appealing for high voltage dc-link EVs and an area of research worth exploring.

Another trend is to minimise the price and size of converters by using an integrated drive motor. Integrating the converter and motor in the same compact package improves the power density with smaller and more efficient electrical components. This solution has multiple advantages, including the reduction and simplification of overall cabling and the resulting reduction in the common mode current. An example of a multiphase integrated drive is presented in [173,174]. The system presented in [173] consists of a 60 kW, nine-phase machine with a max speed of 11500 rpm and a peak torque of 170 Nm, fed by nine half-bridges with nine capacitors connected to a common dc-link voltage source. The nine-phase drivetrain is shown in Figure 32. However, the limitation of this solution is the thermal management and heat dissipation from a mechanical point of view, where generally a liquid cooling system is required in order to dissipate the heat created by machine and inverter losses.

The control of multiphase machines is more complicated and requires more computations compared to a traditional single- or three-phase machine. Significantly, the main challenge is the feasibility and complexity of implementing a control strategy into the digital signal processor (DSP) or microcontroller, taking into account the clock speed and memory limits. An advanced control method should be developed to facilitate the integration of MPDs into industry. The latest trend in industrial manufacturing and monitoring is the "digital twin" (DT) which is currently being defined and explored. It shows promising results in facilitating the control and predictive maintenance concepts by using only data, while no complicated models are needed [175].

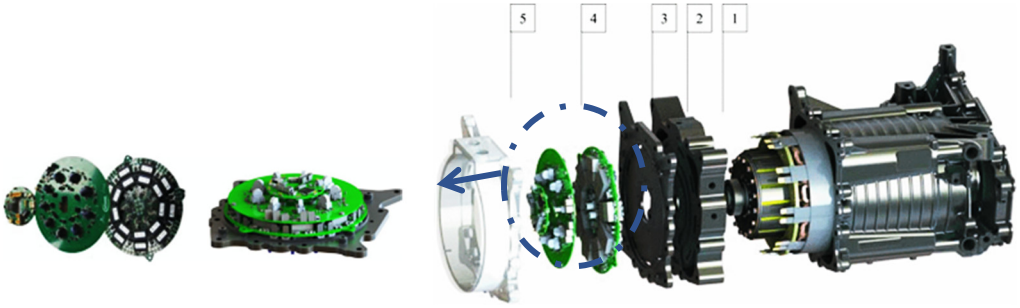

Figure 32. Nine-phase drivetrain for EV applications. (1) Motor housing, (2) Stator, (3) Ferrite motor, (4) Bearing shield-inverter base plate, and (5) Inverter [173].

9. Conclusions

In the past decade, there has been significant progress in the field of multiphase drive technology. Therefore, this paper provides a comprehensive review of the current state of multiphase drives and their use in electric vehicle applications. In this paper, the advantages of using multiphase drives are reviewed and analysed. Moreover, various multiphase electric machine topologies and configurations are presented. Additionally, a general mathematical formulation for multiphase electric machine modelling is covered using coupled *d-q*, decoupled *d-q*, and *VSD* techniques. The paper compares different drive topologies, with a focus on multilevel and reduced-order multiphase drives, based on various factors. The paper also discusses less common drive topologies for multiphase machines, such as multiples of three-phase, seven-phase, and nine-phase machines, as well as various control strategies and modulation techniques that can be used for multiphase drives. Finally, the paper discusses the current state of the market for industrialised multiphase drives and the challenges that must be overcome in terms of reliability and manufacturing costs.

It can be concluded that multiphase drives are a vital enabling technology that is ready to power the future of electric vehicle traction in the coming decades. However, there is still a need for further research in various areas to fully realise this potential. These areas of study could include the development of new multiphase drive topologies and configurations to improve efficiency, reliability, and performance, as well as the investigation of the impact of different operating conditions such as temperature on the performance of these drives. There is also a need for the development of new control algorithms and techniques for multiphase drives to optimize performance and reduce losses, as well as the development of fault diagnosis and fault-tolerant techniques to improve reliability and reduce maintenance requirements for these drives.

It is anticipated that as technology progresses and more research is conducted, the cost of multiphase drives will decrease and the technology and topologies will be enhanced. This is expected to result in an increase in the use of multiphase drives in electric vehicles in the coming years.

Author Contributions: M.A.F. reviewed and wrote the first draft of the paper; J.C. and K.D. contributed to reviewing and editing the paper; Y.B. and M.E.B. reviewed and improved the structure of the paper; and O.H. reviewed and supervised this research study. All authors have read and agreed to the published version of the manuscript.

Funding: This study was funded by a Vrije Universiteit Brussel (VUB) scholarship.

Data Availability Statement: Not applicable.

Acknowledgments: The authors acknowledge the support of Flanders Make for our research group.

Conflicts of Interest: The authors declare no conflict of interest.

Abbreviations

AC	Alternating current
BLDC	Brushless dc electric motor
CB	Cascaded bridge
CBPWM	Carrier based pulse width-modulation
CHB	Cascaded H-bridge converter
CM	Common frequency
CMV	Common-mode voltage
DC	Direct current
DSP	Digital signal processor
DT	Digital-Twin
DTC	Direct torque control
DTP	Dual three-phase
EMC	Electromagnetic compatibility
EMI	Electromagnetic interference
EV	Electric vehicle
FC	Flying capacitor
FLI	Four leg inverter
FOC	Field-oriented control
FPTL	Five-phase two-level
FTC	Fault tolerance control
GaN	Gallium nitride
HEMT	High electron mobility transistor
HEV	Hybrid electric vehicle
HV	High voltage
IGBT	Insulated gate bipolar transistor
IM	Induction machine
LCI	Load-commutated inverter
LS-PWM	Level shifted PWM
LV	Low voltage
MMF	Magnetomotive force
MOSFET	Metal-oxide semiconductor field effect transistor
MPC	Model predictive control
MPD	Multiphase drive
MV	Medium voltage
NPC	Neutral point clamped
NSI	Nine switch inverter
OEW	Open end winding
PCC	Predictive current control
PI	Proportional-Integral
PMSM	Permanent magnet motor
PS-PWM	Phase shifted PWM
PTC	Predictive torque control
PUC	Packed U cell
PWM	Pulse wide modulation
RMS	Root mean square
SCR	Silicon controlled rectifier
SHE	Selective harmonics elimination
SI	Silicon
SiC	Silicon carbide
SMC	Sliding mode control
SPWM	Sinusoidal pulse wide modulation
SVPWM	Space vector pulse wide modulation
THD	Total harmonic distortion
TL-DOV	Three-level dual output voltage
VSC	Voltage source converter
VSD	Vector space decomposition
VSI	Voltage source inverter
VSM	Space vector modulation
WBG	Wide bandgap
ZSI	Zero-sequence injection

References

1. Chakraborty, S.; Kumar, N.M.; Jayakumar, A.; Dash, S.K.; Elangovan, D. Selected Aspects of Sustainable Mobility Reveals Implementable Approaches and Conceivable Actions. *Sustainability* **2021**, *13*, 12918. [CrossRef]
2. Ward, E.; Härer, H. Preliminary investigation of an invertor-fed 5-phase induction motor. *Proc. Inst. Electr. Eng.* **1969**, *116*, 980–984. [CrossRef]
3. Abbas, M.A.; Christen, R.; Jahns, T.M. Six-phase voltage source inverter driven induction motor. *IEEE Trans. Ind. Appl.* **1984**, *5*, 1251–1259. [CrossRef]
4. Fuchs, E.; Rosenberg, L. Analysis of an alternator with two displaced stator windings. *IEEE Trans. Power Appar. Syst.* **1974**, *6*, 1776–1786. [CrossRef]
5. Bodo, N.; Levi, E.; Subotic, I.; Espina, J.; Empringham, L.; Johnson, C.M. Efficiency evaluation of fully integrated on-board EV battery chargers with nine-phase machines. *IEEE Trans. Energy Convers.* **2016**, *32*, 257–266. [CrossRef]
6. Diab, M.S.; Elserougi, A.A.; Abdel-Khalik, A.S.; Massoud, A.M.; Ahmed, S. A nine-switch-converter-based integrated motor drive and battery charger system for EVs using symmetrical six-phase machines. *IEEE Trans. Ind. Electron.* **2016**, *63*, 5326–5335. [CrossRef]
7. Subotic, I.; Bodo, N.; Levi, E.; Jones, M.; Levi, V. Isolated chargers for EVs incorporating six-phase machines. *IEEE Trans. Ind. Electron.* **2015**, *63*, 653–664. [CrossRef]
8. Qiao, M.; Jiang, C.; Zhu, Y.; Li, G. Research on design method and electromagnetic vibration of six-phase fractional-slot concentrated-winding PM motor suitable for ship propulsion. *IEEE Access* **2016**, *4*, 8535–8543. [CrossRef]
9. Zahr, H.; Scuiller, F.; Semail, E. Five-phase SPM machine with electronic pole changing effect for marine propulsion. In Proceedings of the 2016 International Conference on Electrical Systems for Aircraft, Railway, Ship Propulsion and Road Vehicles & International Transportation Electrification Conference (ESARS-ITEC), Toulouse, France, 2–4 November 2016; pp. 1–6.
10. Gritter, D.; Kalsi, S.S.; Henderson, N. Variable speed electric drive options for electric ships. In Proceedings of the IEEE Electric Ship Technologies Symposium, Philadelphia, PA, USA, 25–27 July 2005; pp. 347–354.
11. Ådnanes, A.K. *Maritime Electrical Installations and Diesel Electric Propulsion*; ABB Ltd: Zürich, Switzerland, 2003.
12. Corzine, K.; Lu, S. Comparison of hybrid propulsion drive schemes. In Proceedings of the IEEE Electric Ship Technologies Symposium, Philadelphia, PA, USA, 25–27 July 2005; pp. 355–362.
13. Lu, S.; Corzine, K. Multilevel multi-phase propulsion drives. In Proceedings of the IEEE Electric Ship Technologies Symposium, Philadelphia, PA, USA, 25–27 July 2005; pp. 363–370.
14. Papastergiou, K.; Wheeler, P.; Clare, J. Comparison of losses in multilevel converters for aerospace applications. In Proceedings of the 2008 IEEE Power Electronics Specialists Conference, Rhodes, Greece, 15–19 June 2008; pp. 4307–4312.
15. Tahaa, W.; Azerb, P.; Callegaro, A.D.; Emadi, A. Multiphase traction inverters: State-of-the-art review and future trends. *IEEE Access* **2022**, *10*, 4580–4599. [CrossRef]
16. Salem, A.; Narimani, M. A review on multiphase drives for automotive traction applications. *IEEE Trans. Transp. Electrif.* **2019**, *5*, 1329–1348. (In English) [CrossRef]
17. Levi, E. Multiphase electric machines for variable-speed applications. *IEEE Trans. Ind. Electron.* **2008**, *55*, 1893–1909. [CrossRef]
18. Liu, Z.; Li, Y.; Zheng, Z. A review of drive techniques for multiphase machines. *CES Trans. Electr. Mach. Syst.* **2018**, *2*, 243–251. [CrossRef]
19. Levi, E.; Bodo, N.; Dordevic, O.; Jones, M. Recent advances in power electronic converter control for multiphase drive systems. In Proceedings of the 2013 IEEE Workshop on Electrical Machines Design, Control and Diagnosis (WEMDCD), Paris, France, 11–12 March 2013; pp. 158–167.
20. Barrero, F.; Duran, M.J. Recent advances in the design, modeling, and control of multiphase machines—Part I. *IEEE Trans. Ind. Electron.* **2015**, *63*, 449–458. [CrossRef]
21. Levi, E.; Bojoi, R.; Profumo, F.; Toliyat, H.; Williamson, S. Multiphase induction motor drives-a technology status review. *IET Electr. Power Appl.* **2007**, *1*, 489–516. [CrossRef]
22. Parsa, L. On advantages of multi-phase machines. In Proceedings of the 31st Annual Conference of IEEE Industrial Electronics Society, Raleigh, NC, USA, 6–10 November 2005; p. 6.
23. Baneira, F.; Doval-Gandoy, J.; Yepes, A.G.; Lopez, O.; Pérez-Estévez, D. Control strategy for multiphase drives with minimum losses in the full torque operation range under single open-phase fault. *IEEE Trans. Power Electron.* **2016**, *32*, 6275–6285. [CrossRef]
24. Munim, W.N.W.A.; Duran, M.J.; Che, H.S.; Bermudez, M.; Gonzalez-Prieto, I.; Rahim, N.A. A unified analysis of the fault tolerance capability in six-phase induction motor drives. *IEEE Trans. Power Electron.* **2016**, *32*, 7824–7836. [CrossRef]
25. Wang, X.; Wang, Z.; Xu, Z.; Cheng, M.; Wang, W.; Hu, Y. Comprehensive diagnosis and tolerance strategies for electrical faults and sensor faults in dual three-phase PMSM drives. *IEEE Trans. Power Electron.* **2018**, *34*, 6669–6684. [CrossRef]
26. Che, H.S.; Duran, M.J.; Levi, E.; Jones, M.; Hew, W.-P.; Rahim, N.A. Postfault operation of an asymmetrical six-phase induction machine with single and two isolated neutral points. *IEEE Trans. Power Electron.* **2013**, *29*, 5406–5416. [CrossRef]
27. Yepes, A.G.; Doval-Gandoy, J.; Baneira, F.; Toliyat, H. Postfault strategy for dual three-phase machines with minimum loss in the full torque operation range under two open phases. In Proceedings of the 2018 IEEE Energy Conversion Congress and Exposition (ECCE), Portland, OR, USA, 23–27 September 2018; pp. 3380–3385.
28. Fu, J.-R.; Lipo, T.A. Disturbance-free operation of a multiphase current-regulated motor drive with an opened phase. *IEEE Trans. Ind. Appl.* **1994**, *30*, 1267–1274.

29. Zhao, Y.; Lipo, T.A. Space vector PWM control of dual three-phase induction machine using vector space decomposition. *IEEE Trans. Ind. Appl.* **1995**, *31*, 1100–1109. [CrossRef]
30. Zhao, Y.; Lipo, T.A. Modeling and control of a multi-phase induction machine with structural unbalance Part I. Machine Modeling and Multi-Dimensional Current Regulation. *IEEE Trans. Energy Convers.* **1996**, *11*, 578–584. [CrossRef]
31. Che, H.S.; Levi, E.; Jones, M.; Hew, W.-P.; Rahim, N.A. Current control methods for an asymmetrical six-phase induction motor drive. *IEEE Trans. Power Electron.* **2013**, *29*, 407–417. [CrossRef]
32. Divan, D. Low stress switching for efficiency. *IEEE Spectrum* **1996**, *33*, 33–39. [CrossRef]
33. Stemmler, H.; Guggenbach, P. Configurations of high-power voltage source inverter drives. In Proceedings of the 1993 Fifth European Conference on Power Electronics and Applications, Brighton, UK, 13–16 September 1993; pp. 7–14.
34. Kouro, S.; Malinowski, M.; Gopakumar, K.; Pou, J.; Franquelo, L.G.; Wu, B.; Rodriguez, J.; Pérez, M.A.; Leon, J.I. Recent advances and industrial applications of multilevel converters. *IEEE Trans. Ind. Electron.* **2010**, *57*, 2553–2580. [CrossRef]
35. Rodríguez, J.; Bernet, S.; Wu, B.; Pontt, J.O.; Kouro, S. Multilevel voltage-source-converter topologies for industrial medium-voltage drives. *IEEE Trans. Ind. Electron.* **2007**, *54*, 2930–2945. [CrossRef]
36. Kouro, S.; Rodriguez, J.; Wu, B.; Bernet, S.; Perez, M. Powering the future of industry: High-power adjustable speed drive topologies. *IEEE Ind. Appl. Mag.* **2012**, *18*, 26–39. [CrossRef]
37. Corzine, K.; Sudhoff, S.; Whitcomb, C. Performance characteristics of a cascaded two-level converter. *IEEE Trans. Energy Convers.* **1999**, *14*, 433–439. [CrossRef]
38. Duran, M.J.; Gonzalez-Prieto, I.; Rios-Garcia, N.; Barrero, F. A simple, fast, and robust open-phase fault detection technique for six-phase induction motor drives. *IEEE Trans. Power Electron.* **2017**, *33*, 547–557. [CrossRef]
39. Baneira, F.; Doval-Gandoy, J.; Yepes, A.G.; Lopez, O.; Pérez-Estévez, D. Comparison of postfault strategies for current reference generation for dual three-phase machines in terms of converter losses. *IEEE Trans. Power Electron.* **2017**, *32*, 8243–8246. [CrossRef]
40. Negahdari, A.; Yepes, A.G.; Doval-Gandoy, J.; Toliyat, H.A. Efficiency enhancement of multiphase electric drives at light-load operation considering both converter and stator copper losses. *IEEE Trans. Power Electron.* **2018**, *34*, 1518–1525. [CrossRef]
41. Lyra, R.O.; Lipo, T.A. Torque density improvement in a six-phase induction motor with third harmonic current injection. *IEEE Trans. Ind. Appl.* **2002**, *38*, 1351–1360. [CrossRef]
42. Bendixen, F.B.; Blaabjerg, F.; Rasmussen, P.O.; Vadstrup, P.; Krabbe, K. Controlling the DC-link midpoint potential in a six-phase motor-drive. In Proceedings of the 2004 IEEE 35th Annual Power Electronics Specialists Conference (IEEE Cat. No. 04CH37551), Aachen, Germany, 20–25 June 2004; Volume 3, pp. 2128–2132.
43. Abdel-Khalik, A.S.; Gadoue, S.M.; Masoud, M.I.; Wiliams, B.W. Optimum flux distribution with harmonic injection for a multiphase induction machine using genetic algorithms. *IEEE Trans. Energy Convers.* **2011**, *26*, 501–512. [CrossRef]
44. Abdel-Khalik, A.S.; Gadoue, S.M. Improved flux pattern by third harmonic injection for multiphase induction machines using neural network. *Alex. Eng. J.* **2011**, *50*, 163–169. [CrossRef]
45. Wang, K.; Zhu, Z.; Ren, Y.; Ombach, G. Torque improvement of dual three-phase permanent-magnet machine with third-harmonic current injection. *IEEE Trans. Ind. Electron.* **2015**, *62*, 6833–6844. [CrossRef]
46. Hu, Y.; Zhu, Z.Q.; Odavic, M. Torque capability enhancement of dual three-phase PMSM drive with fifth and seventh current harmonics injection. *IEEE Trans. Ind. Appl.* **2017**, *53*, 4526–4535. [CrossRef]
47. Feng, G.; Lai, C.; Kelly, M.; Kar, N.C. Dual three-phase PMSM torque modeling and maximum torque per peak current control through optimized harmonic current injection. *IEEE Trans. Ind. Electron.* **2018**, *66*, 3356–3368. [CrossRef]
48. Nie, Z. Multiphase Power Electronic Converters for Electric Vehicle Machine Drive Systems. Ph.D. Dissertation, Department of Electrical & Computer Engineering - McMaster University, Hamilton, ON, Canada, 2018.
49. da Rosa, R.S.; Pereira, L.A.; Pereira, L.F.; Haffner, S. Comparison of operating curves of five-phase and three-phase induction machines of same size. In Proceedings of the IECON 2014-40th Annual Conference of the IEEE Industrial Electronics Society, Dallas, TX, USA, 29 October–1 November 2014; pp. 450–455.
50. Nekoubin, A.; Soltani, J.; Dowlatshahi, M. Comparative analysis of three-phase and five-phase permanent-magnet motor based on finite element method. *J. Electr. Eng. Technol.* **2020**, *15*, 1705–1712. [CrossRef]
51. Khan, K.S.; Arshad, W.M.; Kanerva, S. On performance figures of multiphase machines. In Proceedings of the 2008 18th International Conference on Electrical Machines, Vilamoura, Portugal, 6–9 September 2008; pp. 1–5.
52. Boglietti, A.; Bojoi, R.; Cavagnino, A.; Tenconi, A. Efficiency analysis of PWM inverter fed three-phase and dual three-phase induction machines. In Proceedings of the Conference Record of the 2006 IEEE Industry Applications Conference Forty-First IAS Annual Meeting, Tampa, FL, USA, 8–12 October 2006; Volume 1, pp. 434–440.
53. Boglietti, A.; Bojoi, R.; Cavagnino, A.; Tenconi, A. Efficiency analysis of PWM inverter fed three-phase and dual three-phase high frequency induction machines for low/medium power applications. *IEEE Trans. Ind. Electron.* **2008**, *55*, 2015–2023. [CrossRef]
54. Eldeeb, H.M.; Abdel-Khalik, A.S.; Hackl, C.M. Postfault full torque–speed exploitation of dual three-phase IPMSM drives. *IEEE Trans. Ind. Electron.* **2018**, *66*, 6746–6756. [CrossRef]
55. Karttunen, J.; Kallio, S.; Peltoniemi, P.; Silventoinen, P.; Pyrhönen, O. Dual three-phase permanent magnet synchronous machine supplied by two independent voltage source inverters. In Proceedings of the International Symposium on Power Electronics Power Electronics, Electrical Drives, Automation and Motion, Sorrento, Italy, 20–22 June 2012; pp. 741–747.
56. Kallio, S.; Andriollo, M.; Tortella, A.; Karttunen, J. Decoupled dq model of double-star interior-permanent-magnet synchronous machines. *IEEE Trans. Ind. Electron.* **2012**, *60*, 2486–2494. [CrossRef]

57. Baker, R.H. High-Voltage Converter Circuit. U.S. Patent No. 4,203,151, 13 May 1980.
58. Nabae, A.; Takahashi, I.; Akagi, H. A new neutral-point-clamped PWM inverter. *IEEE Trans. Ind. Appl.* **1981**, *5*, 518–523. [CrossRef]
59. Baker, R.H. Bridge Converter Circuit. U.S. Patent No. 4,270,163, 26 May 1981.
60. Lopez, I.; Ceballos, S.; Pou, J.; Zaragoza, J.; Andreu, J.; Kortabarria, I.; Agelidis, V.G. Modulation strategy for multiphase neutral-point-clamped converters. *IEEE Trans. Power Electron.* **2015**, *31*, 928–941. [CrossRef]
61. Gao, L.; Fletcher, J.E. A space vector switching strategy for three-level five-phase inverter drives. *IEEE Trans. Ind. Electron.* **2009**, *57*, 2332–2343.
62. Chikondra, B.; Muduli, U.R.; Behera, R.K. Performance comparison of five-phase three-level npc to five-phase two-level vsi. *IEEE Trans. Ind. Appl.* **2020**, *56*, 3767–3775. [CrossRef]
63. Dordevic, O.; Jones, M.; Levi, E. A comparison of carrier-based and space vector PWM techniques for three-level five-phase voltage source inverters. *IEEE Trans. Ind. Inform.* **2012**, *9*, 609–619. [CrossRef]
64. Fracchia, M.; Ghiara, T.; Marchesoni, M.; Mazzucchelli, M. Optimized modulation techniques for the generalized N-level converter. In Proceedings of the PESC'92 Record. In Proceedings of the 23rd Annual IEEE Power Electronics Specialists Conference, Toledo, Spain, 29 June–3 July 1992; pp. 1205–1213.
65. Bruckner, T.; Bernet, S.; Guldner, H. The active NPC converter and its loss-balancing control. *IEEE Trans. Ind. Electron.* **2005**, *52*, 855–868. [CrossRef]
66. Busquets-Monge, S.; Alepuz, S.; Bordonau, J.; Peracaula, J. Voltage balancing control of diode-clamped multilevel converters with passive front-ends. *IEEE Trans. Power Electron.* **2008**, *23*, 1751–1758. [CrossRef]
67. Steimer, P.; Odegard, B.; Apeldoorn, O.; Bernet, S.; Bruckner, T. Very high power IGCT PEBB technology. In Proceedings of the 2005 IEEE 36th Power Electronics Specialists Conference, Dresden, Germany, 16 June 2005; pp. 1–7.
68. Apeldoorn, O.; Odegard, B.; Steimer, P.; Bernet, S. A 16 mva anpc-pebb with 6 ka igcts. In Proceedings of the Fourtieth IAS Annual Meeting. Conference Record of the 2005 Industry Applications Conference, Hong Kong, China, 2–6 October 2005; Volume 2, pp. 818–824.
69. Dickerson, J.A.; Ottaway, G.H. Transformerless Power Supply with Line to Load Isolation. U.S. Patent 3,596,369, 3 August 1971.
70. Rodriguez, J.; Franquelo, L.G.; Kouro, S.; Leon, J.I.; Portillo, R.C.; Prats MA, M.; Perez, M.A. Multilevel converters: An enabling technology for high-power applications. *Proc. IEEE* **2009**, *97*, 1786–1817. [CrossRef]
71. Darijevic, M.; Jones, M.; Levi, E. An open-end winding four-level five-phase drive. *IEEE Trans. Ind. Electron.* **2015**, *63*, 538–549. [CrossRef]
72. Dhanamjayulu, C.; Sanjeevikumar, P.; Muyeen, S. A structural overview on transformer and transformer-less multi level inverters for renewable energy applications. *Energy Rep.* **2022**, *8*, 10299–10333.
73. Narasipuram, R.P.; Yadlapalli, R.T. Performance analysis and design optimisation of 3-⌀ Packed U Cell inverter for industrial drive applications. *Int. J. Math. Model. Numer. Optim.* **2019**, *9*, 309–337. [CrossRef]
74. Dhanamjayulu, C.; Prasad, D.; Padmanaban, S.; Maroti, P.K.; Holm-Nielsen, J.B.; Blaabjerg, F. Design and implementation of seventeen level inverter with reduced components. *IEEE Access* **2021**, *9*, 16746–16760. [CrossRef]
75. Dwivedi, D.; Roy, I.; Chinmaya, K. Investigation of Three-level Dual Output T-type NPC for EV Application. In Proceedings of the 2022 International Conference on Smart Energy Systems and Technologies (SEST), Eindhoven, The Netherlands, 5–7 September 2022; pp. 1–6.
76. Guennegues, V.; Gollentz, B.; Leclere, L.; Meibody-Tabar, F.; Rael, S. Selective harmonic elimination PWM applied to H-bridge topology in high speed applications. In Proceedings of the 2009 International Conference on Power Engineering, Energy and Electrical Drives, Lisbon, Portugal, 18–20 March 2009; pp. 152–156.
77. Cheng, Z.; Wu, B. A novel switching sequence design for five-level NPC/H-bridge inverters with improved output voltage spectrum and minimized device switching frequency. *IEEE Trans. Power Electron.* **2007**, *22*, 2138–2145. [CrossRef]
78. Wu, C.; Lau, W.H.; Chung, H. A five-level neutral-point-clamped H-bridge PWM inverter with superior harmonics suppression: A theoretical analysis. In Proceedings of the 1999 IEEE International Symposium on Circuits and Systems (ISCAS), Orlando, FL, USA, 30 May–2 June 1999; Volume 5, pp. 198–201.
79. Guennegues, V.; Gollentz, B.; Meibody-Tabar, F.; Raël, S.; Leclere, L. A converter topology for high speed motor drive applications. In Proceedings of the 2009 13th European Conference on Power Electronics and Applications, Barcelona, Spain, 8–10 September 2009; pp. 1–8.
80. Gemmell, B.; Dorn, J.; Retzmann, D.; Soerangr, D. Prospects of multilevel VSC technologies for power transmission. In Proceedings of the 2008 IEEE/PES Transmission and Distribution Conference and Exposition, Chicago, IL, USA, 21–24 April 2008; pp. 1–16.
81. Marquardt, R. A new modular voltage source inverter topology. *Conf. Rec. 10th EPE* **2003**, 1–10.
82. Glinka, M. Prototype of multiphase modular-multilevel-converter with 2 MW power rating and 17-level-output-voltage. In Proceedings of the 2004 IEEE 35th Annual Power Electronics Specialists Conference (IEEE Cat. No. 04CH37551), Aachen, Germany, 20–25 June 2004; Volume 4, pp. 2572–2576.
83. Santos, E.D.; Jacobina, C.; Da Silva, O. Six-phase machine drive system with nine-switch converter. In Proceedings of the IECON 2011-37th Annual Conference of the IEEE Industrial Electronics Society, Melbourne, VIC, Australia, 7–10 November 2011; pp. 4204–4209.

84. Gao, F.; Zhang, L.; Li, D.; Loh, P.C.; Tang, Y.; Gao, H.L. Optimal Pulsewidth Modulation of Nine-Switch Converter. *IEEE Trans. Power Electron.* **2010**, *25*, 2331–2343. (In English) [CrossRef]
85. Goyal, G.N.; Aware, M.V. A comparative performance of six-phase nine switch inverter operation with SPWM and SVPWM. In Proceedings of the 2012 IEEE International Conference on Power Electronics, Drives and Energy Systems (PEDES), Bengaluru, India, 16–19 December 2012; pp. 1–6.
86. Salem, A.S.; Hamdy, R.A.; Abdel-Khalik, A.S.; El-Arabawy, I.F.; Hamad, M.S. Performance of nine-switch inverter-fed asymmetrical six-phase induction machine under machine and converter faults. In Proceedings of the 2016 Eighteenth International Middle East Power Systems Conference (MEPCON), Cairo, Egypt, 27–29 December 2016; pp. 711–716.
87. Guazzelli, P.R.; de Castro, A.G.; dos Santos, S.T.; de Oliveira, C.M.; Pereira, W.C.; Monteiro, J.R.; de Aguiar, M.L. Dual predictive current control of grid connected nine-switch converter applied to induction generator. In Proceedings of the 2018 13th IEEE International Conference on Industry Applications (INDUSCON), Sao Paulo, Brazil, 12–14 November 2018; pp. 1038–1044.
88. Gulbudak, O.; Gokdag, M. Predictive dual-induction machine control using nine-switch inverter for multi-drive systems. In Proceedings of the 2018 IEEE 12th International Conference on Compatibility, Power Electronics and Power Engineering (CPE-POWERENG 2018), Doha, Qatar, 10–12 April 2018; pp. 1–6.
89. Sharma, S.; Aware, M.; Bhowate, A. Direct torque control of symmetrical six-phase induction machine using nine switch inverter. In Proceedings of the 2017 IEEE Transportation Electrification Conference (ITEC-India), Pune, India, 13-15 December 2017; pp. 1–6.
90. Abbache, M.; Tabbache, B.; Kheloui, A. Direct torque control of nine switches inverter—Dual induction motors. In Proceedings of the 22nd Mediterranean Conference on Control and Automation, Palermo, Italy, 16–19 June 2014; pp. 810–815.
91. Oka, K.; Nozawa, Y.; Matsuse, K. Improved method of voltage utility factor for PWM control method of five-leg inverter. In Proceedings of the 2006 37th IEEE Power Electronics Specialists Conference, Jeju, Republic of Korea, 18–22 June 2006; pp. 1–5.
92. Jacobina, C.B.; de Freitas, I.S.; da Silva, C.R.; de Rossiter Correa, M.B.; da Silva, E.R.C. Reduced switch-count six-phase AC motor drive systems without input reactor. *IEEE Trans. Ind. Electron.* **2008**, *55*, 2024–2032. [CrossRef]
93. Oka, K.; Nozawa, Y.; Omata, R.; Suzuki, K.; Furuya, A.; Matsuse, K. Characteristic comparison between five-leg inverter and nine-switch inverter. In Proceedings of the 2007 Power Conversion Conference-Nagoya, Nagoya, Japan, 2–5 April 2007; pp. 279–283.
94. Jing, G.; Zhou, C. Control strategy for a five-leg inverter supplying dual three-phase PMSM. *IEEE Access* **2020**, *8*, 174480–174488. [CrossRef]
95. Wei, J.; Zhang, T.; Liu, P.; Tao, W.; Zhou, B. Investigation of a fault-tolerant control method for a multiport dual-stator doubly salient electromagnetic machine drive. *IEEE Trans. Ind. Electron.* **2018**, *66*, 750–761. [CrossRef]
96. Furuya, A.; Oka, K.; Matsuse, K. A characteristic analysis of four-leg inverter in two AC motor drives with independent vector control. In Proceedings of the 2007 International Conference on Electrical Machines and Systems (ICEMS), Seoul, Republic of Korea, 8–11 October 2007; pp. 619–624.
97. Oka, K. Independent vector control of two induction motors with a four-leg inverter by the expanded two arm modulation method. *Acad. Manag. Rev.* 2005 National Convention Record IEEJ, No. 4-129. **2005**, 201–202.
98. Oka, K.; Matsuse, K. A performance analysis of a four-leg inverter in two AC motor drives with independent vector control. *IEEJ Trans. Electr. Electron. Eng.* **2006**, *1*, 104–107. [CrossRef]
99. Bodo, N.; Jones, M.; Levi, E. A space vector PWM with common-mode voltage elimination for open-end winding five-phase drives with a single DC supply. *IEEE Trans. Ind. Electron.* **2013**, *61*, 2197–2207. [CrossRef]
100. Azeez, N.A.; Mathew, J.; Gopakumar, K.; Cecati, C. A 5th and 7th order harmonic suppression scheme for open-end winding asymmetrical six-phase IM drive using capacitor-fed inverter. In Proceedings of the IECON 2013-39th Annual Conference of the IEEE Industrial Electronics Society, Vienna, Austria, 10–13 November 2013; pp. 5118–5123.
101. Mohapatra, K.; Gopakumar, K. A novel split phase induction motor drive without harmonic filters and with linear voltage control for the full modulation range. *EPE J.* **2006**, *16*, 20–28. [CrossRef]
102. Jones, M.; Patkar, F.; Levi, E. Carrier-based pulse-width modulation techniques for asymmetrical six-phase open-end winding drives. *IET Electr. Power Appl.* **2013**, *7*, 441–452. [CrossRef]
103. Loncarski, J.; Leijon, M.; Rossi, C.; Srndovic, M.; Grandi, G. Current ripple evaluation in dual three-phase inverters for open-end winding EV drives. In Proceedings of the 2014 International Conference on Connected Vehicles and Expo (ICCVE), Vienna, Austria, 3–7 November 2014; pp. 507–513.
104. Patkar, F.; Jidin, A.; Levi, E.; Jones, M. Performance comparison of symmetrical and asymmetrical six-phase open-end winding drives with carrier-based PWM. In Proceedings of the 2017 6th International Conference on Electrical Engineering and Informatics (ICEEI), Langkawi, Malaysia, 25–27 November 2017; pp. 1–6.
105. Wang, Z.; Chen, J.; Cheng, M. Modeling and control of neutral-point-clamping (NPC) three-level inverters fed dual-three phase PMSM drives. In Proceedings of the 2015 IEEE Energy Conversion Congress and Exposition (ECCE), Montreal, QC, Canada, 20–24 September 2015; pp. 6565–6572.
106. Nair, V.; Pramanick, S.; Gopakumar, K.; Franquelo, L.G. Novel symmetric six-phase induction motor drive using stacked multilevel inverters with a single DC link and neutral point voltage balancing. *IEEE Trans. Ind. Electron.* **2016**, *64*, 2663–2670.
107. Wang, Z.; Wang, X.; Wang, Y.; Chen, J.; Cheng, M. Fault tolerant control of multiphase multilevel motor drives-technical review. *Chin. J. Electr. Eng.* **2017**, *3*, 76–86.

108. Coates, C.; Platt, D.; Gosbell, V. Performance evaluation of a nine-phase synchronous reluctance drive. In Proceedings of theConference Record of the 2001 IEEE Industry Applications Conference. 36th IAS Annual Meeting (Cat. No. 01CH37248), Chicago, IL, USA, 30 September–4 October 2001; Volume 3, pp. 2041–2047.
109. Tawfiq, K.B.; Ibrahim, M.N.; EL-Kholy, E.; Sergeant, P. Performance analysis of a rewound multiphase synchronous reluctance machine. *IEEE J. Emerg. Sel. Top. Power Electron.* **2021**, *10*, 297–309. [CrossRef]
110. Jung, E.; Yoo, H.; Sul, S.-K.; Choi, H.-S.; Choi, Y.-Y. A nine-phase permanent-magnet motor drive system for an ultrahigh-speed elevator. *IEEE Trans. Ind. Appl.* **2012**, *48*, 987–995. [CrossRef]
111. de Souza, T.S.; Bastos, R.R.; Filho, B.J.C. Modeling and control of a nine-phase induction machine with open phases. *IEEE Trans. Ind. Appl.* **2018**, *54*, 6576–6585. [CrossRef]
112. Kummari, J.B.; Keerthipati, S. Operation of nine-phase induction machine under single-phase open-winding fault condition using dodecagonal SVPWM and hexagonal SVPWM. In Proceedings of the IECON 2019-45th Annual Conference of the IEEE Industrial Electronics Society, Lisbon, Portugal, 14–17 October 2019; Volume 1, pp. 3231–3236.
113. Rockhill, A.A.; Lipo, T. A simplified model of a nine-phase synchronous machine using vector space decomposition. *Electr. Power Compon. Syst.* **2010**, *38*, 477–489. [CrossRef]
114. Gerrits, T.; Duarte, J.; Wijnands, C.; Lomonova, E.; Paulides, J.; Encica, L. Twelve-phase open-winding SPMSM development for speed dependent reconfigurable traction drive. In Proceedings of the 2015 Tenth International Conference on Ecological Vehicles and Renewable Energies (EVER), Monte Carlo, Monaco, 31 March–2 April 2015; pp. 1–7.
115. Cho, B.G.; Yoon, Y.D.; Sul, S.K.; Kong, Y.K.; Bin, J.G.; Park, S.J.; Lee, M.L. A separate double-winding 12-phase brushless DC motor drive fed from individual H-bridge inverters. In Proceedings of the 2010 IEEE Energy Conversion Congress and Exposition, Atlanta, GA, USA, 12–16 September 2010; pp. 3889–3895.
116. Sun, C.; Ai, S.; Hu, L.; Chen, Y. The development of a 20MW PWM driver for advanced fifteen-phase propulsion induction motors. *J. Power Electron.* **2015**, *15*, 146–159. [CrossRef]
117. Liu, Z.; Peng, L.; Li, Y.; Zheng, Z.; Wang, K. Modeling and control of 15-phase induction machine under one phase open circuit fault. In Proceedings of the 2013 International Conference on Electrical Machines and Systems (ICEMS), Busan, Republic of Korea, 26–29 October 2013; pp. 2066–2071.
118. Grandi, G.; Serra, G.; Tani, A. Space vector modulation of a seven-phase voltage source inverter. In Proceedings of the International Symposium on Power Electronics, Electrical Drives, Automation and Motion, SPEEDAM, Taormina, Italy, 23–26 May 2006; pp. 1149–1156.
119. Khan, M.A.; Ahmed, S.M.; Iqbal, A.; Rub, H.A.; Moinoddin, S. Discontinuous space vector PWM strategies for a seven-phase voltage source inverter. In Proceedings of the 2009 35th Annual Conference of IEEE Industrial Electronics, Porto, Portugal, 3–5 November 2009; pp. 397–402.
120. Dujic, D.; Levi, E.; Jones, M.; Grandi, G.; Serra, G.; Tani, A. Continuous PWM techniques for sinusoidal voltage generation with seven-phase voltage source inverters. In Proceedings of the 2007 IEEE Power Electronics Specialists Conference, Orlando, FL, USA, 17–21 June 2007; pp. 47–52.
121. Ahmed, S.M.; Iqbal, A.; Abu-Rub, H.; Khan, M.R. Carrier based PWM technique for a novel three-to-seven phase matrix converter. In Proceedings of the XIX International Conference on Electrical Machines-ICEM 2010, Rome, Italy, 6–8 September 2010; pp. 1–6.
122. Dabour, S.M.; Allam, S.; Rashad, E.M. Space vector PWM technique for three-to seven-phase matrix converters. In Proceedings of the 16th International Middle-East Power Systems Conference-MEPCON, Cairo, Egypt, 23–25 December 2014; pp. 1–6.
123. Casadei, D.; Dujic, D.; Levi, E.; Serra, G.; Tani, A.; Zarri, L. General modulation strategy for seven-phase inverters with independent control of multiple voltage space vectors. *IEEE Trans. Ind. Electron.* **2008**, *55*, 1921–1932. [CrossRef]
124. Dordevic, O.; Levi, E.; Jones, M. A vector space decomposition based space vector PWM algorithm for a three-level seven-phase voltage source inverter. *IEEE Trans. Power Electron.* **2012**, *28*, 637–649. [CrossRef]
125. Abdelkhalik, A.; Masoud, M.; Barry, W. Eleven-phase induction machine: Steady-state analysis and performance evaluation with harmonic injection. *IET Electr. Power Appl.* **2010**, *4*, 670–685. [CrossRef]
126. Abdel-Khalik, A.; Masoud, M.; Williams, B. Performance evaluation of eleven-phase induction machine using selective harmonic elimination. In Proceedings of the 2011 International Conference on Power Engineering, Energy and Electrical Drives, Malaga, Spain, 11–13 May 2011; pp. 1–6.
127. Semenov, D.; Tian, B.; An, Q.-T.; Sun, L. Position estimation for sensorless FOC of five-phase PMSM in electric vehicles. In Proceedings of the 2016 Australasian Universities Power Engineering Conference (AUPEC), Brisbane, QLD, Australia, 25–28 September 2016; pp. 1–5.
128. Zhao, Y.; Lipo, T.A. Modeling and control of a multi-phase induction machine with structural unbalance Part II. Field-oriented control and experimental verification. *IEEE Trans. Energy Convers.* **1996**, *11*, 578–584. [CrossRef]
129. Martin, J.-P.; Meibody-Tabar, F.; Davat, B. Multiple-phase permanent magnet synchronous machine supplied by VSIs, working under fault conditions. In Proceedings of the Conference Record of the 2000 IEEE Industry Applications Conference. Thirty-Fifth IAS Annual Meeting and World Conference on Industrial Applications of Electrical Energy (Cat. No. 00CH37129), Rome, Italy, 8–12 October 2000; Volume 3, pp. 1710–1717.
130. Kianinezhad, R.; Nahid-Mobarakeh, B.; Baghli, L.; Betin, F.; Capolino, G.-A. Modeling and control of six-phase symmetrical induction machine under fault condition due to open phases. *IEEE Trans. Ind. Electron.* **2008**, *55*, 1966–1977. [CrossRef]

131. Ryu, H.-M.; Kim, J.-W.; Sul, S.-K. Synchronous-frame current control of multiphase synchronous motor under asymmetric fault condition due to open phases. *IEEE Trans. Ind. Appl.* **2006**, *42*, 1062–1070.
132. Tani, A.; Mengoni, M.; Zarri, L.; Serra, G.; Casadei, D. Control of multiphase induction motors with an odd number of phases under open-circuit phase faults. *IEEE Trans. Power Electron.* **2011**, *27*, 565–577. [CrossRef]
133. Dwari, S.; Parsa, L. Fault-tolerant control of five-phase permanent-magnet motors with trapezoidal back EMF. *IEEE Trans. Ind. Electron.* **2010**, *58*, 476–485. [CrossRef]
134. Locment, F.; Semail, E.; Kestelyn, X. Vectorial approach-based control of a seven-phase axial flux machine designed for fault operation. *IEEE Trans. Ind. Electron.* **2008**, *55*, 3682–3691. [CrossRef]
135. Parsa, L.; Toliyat, H.A. Sensorless direct torque control of five-phase interior permanent-magnet motor drives. *IEEE Trans. Ind. Appl.* **2007**, *43*, 952–959. [CrossRef]
136. Tenconi, A.; Rubino, S.; Bojoi, R. Model predictive control for multiphase motor drives–a technology status review. In Proceedings of the 2018 International Power Electronics Conference (IPEC-Niigata 2018-ECCE Asia), Niigata, Japan, 20–24 May 2018; pp. 732–739.
137. Kouro, S.; Cortés, P.; Vargas, R.; Ammann, U.; Rodríguez, J. Model predictive control—A simple and powerful method to control power converters. *IEEE Trans. Ind. Electron.* **2008**, *56*, 1826–1838. [CrossRef]
138. Cortés, P.; Kazmierkowski, M.P.; Kennel, R.M.; Quevedo, D.E.; Rodríguez, J. Predictive control in power electronics and drives. *IEEE Trans. Ind. Electron.* **2008**, *55*, 4312–4324. [CrossRef]
139. Aciego, J.J.; Prieto, I.G.; Duran, M.J. Model predictive control of six-phase induction motor drives using two virtual voltage vectors. *IEEE J. Emerg. Sel. Top. Power Electron.* **2018**, *7*, 321–330. [CrossRef]
140. Gonzalez-Prieto, I.; Duran, M.J.; Aciego, J.J.; Martin, C.; Barrero, F. Model predictive control of six-phase induction motor drives using virtual voltage vectors. *IEEE Trans. Ind. Electron.* **2017**, *65*, 27–37. [CrossRef]
141. Barrero, F.; Arahal, M.R.; Gregor, R.; Toral, S.; Durán, M.J. A proof of concept study of predictive current control for VSI-driven asymmetrical dual three-phase AC machines. *IEEE Trans. Ind. Electron.* **2009**, *56*, 1937–1954. [CrossRef]
142. Lim, C.; Rahim, N.; Hew, W.; Jones, M.; Levi, E. Model predictive current control of a five-phase induction motor. In Proceedings of the IECON 2011-37th Annual Conference of the IEEE Industrial Electronics Society, Melbourne, VIC, Australia, 7–10 November 2011; pp. 1934–1940.
143. Lim, C.S.; Levi, E.; Jones, M.; Rahim, N.A.; Hew, W.P. FCS-MPC-based current control of a five-phase induction motor and its comparison with PI-PWM control. *IEEE Trans. Ind. Electron.* **2013**, *61*, 149–163. [CrossRef]
144. Guzman, H.; Duran, M.J.; Barrero, F.; Bogado, B.; Toral, S. Speed control of five-phase induction motors with integrated open-phase fault operation using model-based predictive current control techniques. *IEEE Trans. Ind. Electron.* **2013**, *61*, 4474–4484. [CrossRef]
145. Bojoi, R.; Lazzari, M.; Profumo, F.; Tenconi, A. Digital field oriented control for dual three-phase induction motor drives. In Proceedings of the Conference Record of the 2002 IEEE Industry Applications Conference, 37th IAS Annual Meeting (Cat. No. 02CH37344), Pittsburgh, PA, USA, 13–18 October 2002; Volume 2, pp. 818–825.
146. Bojoi, R.; Tenconi, A.; Griva, G.; Profumo, F. Vector control of dual-three-phase induction-motor drives using two current sensors. *IEEE Trans. Ind. Appl.* **2006**, *42*, 1284–1292. [CrossRef]
147. Pandit, J.K.; Aware, M.V.; Nemade, R.V.; Levi, E. Direct torque control scheme for a six-phase induction motor with reduced torque ripple. *IEEE Trans. Power Electron.* **2016**, *32*, 7118–7129. [CrossRef]
148. Sala-Perez, P.; Galceran-Arellano, S.; Montesinos-Miracle, D. A sensorless stable V/f control method for a five-phase PMSM. In Proceedings of the 2013 15th European Conference on Power Electronics and Applications (EPE), Lille, France, 2–6 September 2013; pp. 1–10.
149. Furmanik, M.; Gorel, L.; Rafajdus, P. Field oriented control adjustment for 6-phase permanent magnet synchronous machines. *Transp. Res. Procedia* **2021**, *55*, 919–926. [CrossRef]
150. Ren, Y.; Zhu, Z.-Q. Enhancement of steady-state performance in direct-torque-controlled dual three-phase permanent-magnet synchronous machine drives with modified switching table. *IEEE Trans. Ind. Electron.* **2014**, *62*, 3338–3350. [CrossRef]
151. Salehifar, M.; Arashloo, R.S.; Moreno-Eguilaz, M.; Sala, V.; Romeral, L. Observer-based open transistor fault diagnosis and fault-tolerant control of five-phase permanent magnet motor drive for application in electric vehicles. *IET Power Electron.* **2015**, *8*, 76–87. [CrossRef]
152. Shishehgar, J.; Soltani, J.; Tabrizchi, A.M.; Abjadi, N.R. Direct torque and flux control of speed sensorless five-phase interior permanent magnet motor based on adaptive sliding mode control. In Proceedings of the 5th Annual International Power Electronics, Drive Systems and Technologies Conference (PEDSTC 2014), Tehran, Iran, 5–6 February 2014; pp. 37–42.
153. Abjadi, N.R. Sliding-mode control of a six-phase series/parallel connected two induction motors drive. *ISA Trans.* **2014**, *53*, 1847–1856. [CrossRef] [PubMed]
154. Prieto, J.; Levi, E.; Barrero, F.; Toral, S. Output current ripple analysis for asymmetrical six-phase drives using double zero-sequence injection PWM. In Proceedings of the IECON 2011-37th Annual Conference of the IEEE Industrial Electronics Society, Melbourne, VIC, Australia, 7–10 November 2011; pp. 3692–3697.
155. Reddy, B.V.; Somasekhar, V.T.; Kalyan, Y. Decoupled space-vector PWM strategies for a four-level asymmetrical open-end winding induction motor drive with waveform symmetries. *IEEE Trans. Ind. Electron.* **2011**, *58*, 5130–5141. [CrossRef]

156. Hadiouche, D.; Baghli, L.; Rezzoug, A. Space-vector PWM techniques for dual three-phase AC machine: Analysis, performance evaluation, and DSP implementation. *IEEE Trans. Ind. Appl.* **2006**, *42*, 1112–1122. [CrossRef]
157. Zhou, K.; Wang, D. Relationship between space-vector modulation and three-phase carrier-based PWM: A comprehensive analysis [three-phase inverters]. *IEEE Trans. Ind. Electron.* **2002**, *49*, 186–196. [CrossRef]
158. Rakesh, P.; Narayanan, G. Investigation on zero-sequence signal injection for improved harmonic performance in split-phase induction motor drives. *IEEE Trans. Ind. Electron.* **2016**, *64*, 2732–2741. [CrossRef]
159. Rakesh, P.R.; Narayanan, G. Analysis of sine-triangle and zero-sequence injection modulation schemes for split-phase induction motor drive. *IET Power Electron.* **2016**, *9*, 344–355. [CrossRef]
160. Bojoi, R.; Tenconi, A.; Profumo, F.; Griva, G.; Martinello, D. Complete analysis and comparative study of digital modulation techniques for dual three-phase AC motor drives. In Proceedings of the 2002 IEEE 33rd Annual IEEE Power Electronics Specialists Conference, Proceedings (Cat. No. 02CH37289), Cairns, QLD, Australia, 23–27 June 2002; Volume 2, pp. 851–857.
161. DANA TM4. Available online: https://www.danatm4.com/ (accessed on 21 November 2022).
162. Tron-E. Available online: https://en.tronetek.com/ (accessed on 20 December 2022).
163. PCM. Available online: https://www.pcm.eu/ (accessed on 20 December 2022).
164. GE Power Conversion. Available online: https://www.gepowerconversion.com/ (accessed on 20 December 2022).
165. Eaton. Available online: https://www.eaton.com/ (accessed on 20 December 2022).
166. Bose, B.K. Power electronics and motor drives recent progress and perspective. *IEEE Trans. Ind. Electron.* **2008**, *56*, 581–588. [CrossRef]
167. Bindra, A. Wide-bandgap-based power devices: Reshaping the power electronics landscape. *IEEE Power Electron. Mag.* **2015**, *2*, 42–47. [CrossRef]
168. Shimomura, T.; Numakura, K.; Sato, D.; Hayashi, T. High speed dV/dt control technology for a SiC power module for EV/HEV inverters using a multistage drive circuit. In Proceedings of the 2018 IEEE Energy Conversion Congress and Exposition (ECCE), Portland, OR, USA, 23–27 September 2018; pp. 3542–3546.
169. Liu, J.; Su, W.; Tai, X.; Sun, W.; Gu, L.; Wen, X. Development of an inverter using hybrid SIC power module for EV/HEV applications. In Proceedings of the 2016 19th International Conference on Electrical Machines and Systems (ICEMS), Chiba, Japan, 13–16 November 2016; pp. 1–5.
170. Wang, H.; Jiang, D. Design of high temperature gate driver for SiC MOSFET for EV motor drives. In Proceedings of the 2017 IEEE Transportation Electrification Conference and Expo, Asia-Pacific (ITEC Asia-Pacific), Harbin, China, 7–10 August 2017; pp. 1–6.
171. Hazra, S.; Madhusoodhanan, S.; Moghaddam, G.K.; Hatua, K.; Bhattacharya, S. Design considerations and performance evaluation of 1200-V 100-A SiC MOSFET-based two-level voltage source converter. *IEEE Trans. Ind. Appl.* **2016**, *52*, 4257–4268. [CrossRef]
172. Drive, U.S. *Electrical and Electronics Technical Team Roadmap*; Vehicle Technologies Office: Washington, DC, USA, 2017.
173. Brockerhoff, P.; Schön, W.; Blaha, P.; Václavek, P.; Burkhardt, Y. Disc inverter in highly integrated 9-phase drivetrain for E-mobility. In Proceedings of the 2015 17th European Conference on Power Electronics and Applications (EPE'15 ECCE-Europe), Geneva, Switzerland, 8–10 September 2015; pp. 1–9.
174. Brockerhoff, P.; Ehlgen, T.; Burkhardt, Y.; Lucas, P. Electrical drivetrain without rare earth magnets and integrated inverter with inherent redundancy. In Proceedings of the 2013 3rd International Electric Drives Production Conference (EDPC), Nuremberg, Germany, 29–30 October 2013; pp. 1–7.
175. Falekas, G.; Karlis, A. Digital twin in electrical machine control and predictive maintenance: State-of-the-art and future prospects. *Energies* **2021**, *14*, 5933. [CrossRef]